AFRL-RW-EG-TR-2018-079

Inertial Sensing in Insects: Are Multiple Inertial Measurement Units Involved in Flight Control?

Tom Daniel

Department of Biology University of Washington
Program in Neuroscience
4333 Brooklyn Ave NE
Seattle WA, 98195-1800

July 2017

Final Report

Period of Performance: October 2014–July 2017

AIR FORCE RESEARCH LABORATORY
MUNITIONS DIRECTORATE
WEAPON ENGAGEMENT DIVISION
INTEGRATION SENSING & PROCESSING BRANCH
EGLIN AIR FORCE BASE, FL 32542
AIR FORCE MATERIEL COMMAND
UNITED STATES AIR FORCE

NOTICE AND SIGNATURE PAGE

Using Government drawings, specifications, or other data included in this document for any purpose other than Government procurement does not in any way obligate the U.S. Government. The fact that the Government formulated or supplied the drawings, specifications, or other data does not license the holder or any other person or corporation; or convey any rights or permission to manufacture, use, or sell any patented invention that may relate to them.

Qualified requestors may obtain copies of this report from the Defense Technical Information Center (DTIC) <http://www.dtic.mil/dtic/index.html>.

AFRL-RW-EG-TR-2018-079 HAS BEEN REVIEWED AND IS APPROVED FOR PUBLICATION IN ACCORDANCE WITH ASSIGNED DISTRIBUTION STATEMENT.

FOR THE DIRECTOR:

//SIGNED//	**//SIGNED//**
MARTIN (RIC) WEHLING, DR-IV	TIMOTHY KLAUSUTIS, DR-IV, PhD
AFRL/RWWI Program Manager	Terminal Seeker Science CTC Lead

This report is published in the interest of scientific and technical information exchange, and its publication does not constitute the Government's approval or disapproval of its ideas or findings.

REPORT DOCUMENTATION PAGE

Form Approved
OMB No. 0704-0188

1. REPORT DATE *(DD-MM-YYYY)*	**2. REPORT TYPE**	**3. DATES COVERED** ***(From–To)***
05-07-2017	Final	15-10-2014–05-07-2017

4. TITLE AND SUBTITLE

Inertial Sensing in Insects: Are Multiple Inertial Measurement Units Involved in Flight Control?

5a. CONTRACT NUMBER

FA8651-13-1-0004

5b. GRANT NUMBER

N/A

5c. PROGRAM ELEMENT NUMBER

602602F

6. AUTHOR(S)

Tom Daniel

5d. PROJECT NUMBER

N/A

5e. TASK NUMBER

20688718

5f. WORK UNIT NUMBER

W0NP

7. PERFORMING ORGANIZATION NAME(S) AND ADDRESS(ES)

Department of Biology University of Washington
Program in Neuroscience
4333 Brooklyn Ave NE
Seattle WA, 98195-1800

8. PERFORMING ORGANIZATION REPORT NUMBER

N/A

9. SPONSORING/MONITORING AGENCY NAME(S) AND ADDRESS(ES)

Department of the Air Force
Air Force Materiel Command
AFRL—Eglin Research Site
101 West Eglin Blvd
Eglin AFB FL, 32542-6864

10. SPONSOR/MONITOR'S ACRONYM(S)

AFRL/RWWI

11. SPONSOR/MONITOR'S REPORT NUMBER(S)

AFRL-RW-EG-TR-2018-079

12. DISTRIBUTION/AVAILABILITY STATEMENT

DISTRIBUTION A. Approved for public release: distribution unlimited. 96TW-2019-0043.

13.SUPPLEMENTARY NOTES

14. ABSTRACT

This effort is part of a multi-pronged project aimed at understanding the role of mechanosensory information processing for insect flight control. Little is known about the mechanosensory information coming from wings, legs, abdomen, antennae, and head motions, or how it is used. We focused on two mechanosensory systems: (1) distributed wing strain sensors (campaniform sensilla) and (2) abdominal proprioceptive input. The former sensors were a subject of some preliminary research using behavioral studies, intracellular recording methods, and both light and electron microscopy. The latter subject is, as far as we know, unexplored and there is no clear literature on this topic. Both systems are best described as sensing actuators (i.e., "sensuators") that both direct changes in the body trajectory and report changes in the body trajectory.

15. SUBJECT TERMS

insect flight control, mechanosensory, campaniform sensilla, proprioception, abdominal flight control, sensing actuator

16. SECURITY CLASSIFICATION OF:			**17. LIMITATION OF ABSTRACT**	**18. NUMBER OF PAGES**	**19a. NAME OF RESPONSIBLE PERSON**
					MARTIN (RIC) WEHLING
a. REPORT	**b. ABSTRACT**	**c. THIS PAGE**	SAR	53	**19b. TELEPHONE NUMBER** ***with area code***
UNCLASSIFIED	UNCLASSIFIED	UNCLASSIFIED			850-875-1880

Standard Form 298 (Rev. 8-98)
Prescribed by ANSI Std. Z39.18

THIS PAGE INTENTIONALLY LEFT BLANK

TABLE OF CONTENTS

1 OVERVIEW

This research grant revolved around a multi-pronged project aimed at understanding the role of mechanosensory information processing for insect flight control. In contrast to extensive prior work on the role of visual information processing for flight control (e.g., optic flow, horizon tracking, object avoidance) and gyroscopic sensing in dipteran systems (e.g., haltere dynamics) far less is known about the mechanosensory information received via wings, legs, abdomen, antennae, and even head motions. These structures may provide parallel channels of information about the inertial dynamics of the entire animal as it is subjected to perturbations in its trajectory, but relatively little is known about how that information is used by the animal. Importantly, all of these structures are either actively moved or indirectly subjected to oscillations driven by wing inertial dynamics. Thus, all have the capability of providing sensory information for both simple inertial reactions and more complex Coriolis forces. In the case of wings, they may serve both a sensory and an actuator function; through the process of flapping flight, wing motions necessarily also provide gyroscopic information (Daniel et al., 2012). Similarly, the abdomen is critically involved in flight control via shifts in the mass distribution relative to the center of lift (Dyhr et al., 2012).

We focused on two mechanosensory systems: (1) distributed wing strain sensors (campaniform sensilla) and (2) abdominal proprioceptive input. The former sensors were a subject of some preliminary research using behavioral studies, intracellular recording methods, and both light and electron microscopy. The latter subject is, as far as we know, unexplored and there is no clear literature on this topic. Both systems are best described as sensing actuators (*i.e.* “sensuators”) that both direct changes in the body trajectory and report changes in the body trajectory.

2 RESEARCH PRODUCTIVITY

Over the course of this research project (2014–2017), we published 11 peer-reviewed manuscripts related to this grant. In addition, we contributed 23 papers that were presented at international meetings. A detailed list of these papers and conference proceedings can be found in Sections 9 and 10 of this paper. The majority of the contributed talks were presented at the annual meetings of the Society for Integrative and Comparative Biology (SICB).

Because the research launched more projects than could be completed during the course of the grant, we still have a few more manuscripts and presentations that will continue past the end date of the grant. Details of these are described below.

3 PERSONNEL

The grant provided partial support for three postdoctoral trainees (sequentially). Interestingly, each ended up receiving independent support, making room for others to become involved in the research. As such, we also supported four graduate and post-baccalaureate students and two undergraduate students.

Many individuals who worked on the project received funds from other sources (e.g., NSF Graduate Research Fellowships, UW Institute of Neuroengineering, and the AFOSR Center of Excellence). Five graduate students (Bradley Dickerson, Annika Eberle, Thomas Mohren, Mark Jankauski, and Jorge Bustamante) worked on aspects of the research, but all had support from independent fellowships.

4 BROADER IMPACTS

Several high school students (Neil Chauhan, Jane Woods, Emma LaMarka, Luca Scheuer, and Marissa Dominquez) were involved in the research project, all of whom were co-authors of our contributed talks for the various SICB meetings. All were admitted to undergraduate programs of their choice.

Several participants in the research (Elischa Sanders, Darren Howell, Brad Dickerson, Jorge Bustamante, and Kit Githinji) come from underrepresented groups. Dr. Dickerson defended his thesis in 2015 and has been awarded an NSF postdoctoral fellowship to work with Michael Dickinson at Caltech. Darren Howell graduated with a BS in Neurobiology and is joining a laboratory in the UW School of Medicine. Elischa Sanders graduated with a BS in Neurobiology and is joining the MD/PhD program at UC San Diego. Kit Githinji will be graduating with a degree in Electrical Engineering and is heading to the NASA Space Center in Houston as an intern.

5 EXTENSIONS OF THE RESEARCH

The creation of the Air Force Center of Excellence on Nature Inspired Flight Technologies and Ideas[1] owes its origins, in part, to many of the activities associated with this research. The early publications derived from this research program provided critical background for ideas that now are a central part of the COE. Among these are the notions of distributed wing strain sensing for controls, sensed actuators, sparse sensing, and neural filters.

The work done in this grant also formed a key part of our new UW Institute of Neuroengineering. This is supported by a gift from the Washington Research Foundation. Its goal is to build a highly collaborative environment that brings together faculty, students, and staff from the entire University of Washington campus to solve some of the greatest scientific challenges related to neural system function. We aim to provide new assistive device technologies that improve quality of life, to develop neuro-inspired systems that spur the next generation of robotics and autonomous systems, and to foster a deeper understanding of neural system function.

6 WING SENSING AND ACTUATION

Over the past year, we embarked on a series of computational and experimental studies of wing strain sensing, partially funded by this program and by a grant from the AFOSR. The overarching result is that we have accumulated increasing evidence that wings serve the dual function of actuation and gyroscopic sensing. Clearly, wings provide lift and thrust forces. However, because their flapping motions lead to Coriolis forces when combined with body rotations, mechanosensory cells on the wings allow these structures to serve as gyroscopic organs.

1. In Dickerson et al. (2014) we used a combination of electrophysiological and behavioral experiments to show that mechanosensory input to wings subjected to a mechanical stimulus that mimics pitching motions drives a reflexive response identical to that seen for both visual and whole body pitch responses.
2. In Eberle et al., (2013) we developed a computational analysis that explores fluid structure interaction in flapping wings. We showed that structural, not aerodynamic, features dominate the emergent bending dynamics of wings.
3. In Brunton et al. (2014) we used a combination of computational methods associated with sparse sensing, along with neural encoding, to demonstrate optimal sensor placement on wings for detecting Coriolis forces. That work also shows that we can use neural encoding approaches to provide an efficient method for dimension reduction of temporally varying signals.
4. In Eberle et al. (2015) we showed that Coriolis forces on wings lead to wing twisting, and that the shear strains associated with twisting can provide a mechanism for detecting body rotations.

[1] http://nifti.washington.edu

5. In Pratt et al. (2017) we used multi-site extracellular electrode methods to more fully characterize the encoding properties of wing strain sensors. This project sought to unravel the specific features of wing deformation that are encoded by strain sensors (Sanders et al., 2014) and relied on the fact that wing mechanosensory cells are also temperature-sensitive. We used a laser to scan the surface of the wing while simultaneously recording from the sensory neurons in the wing nerve. Using spike sorting algorithms, we identified single units and their locations. With the multi-site electrode still in place, we then mechanically stimulated the wing while simultaneously recording from the wing nerve. Again using spike sorting, we identified units that are strain-sensitive. Importantly, this project allowed us to extract the stimulus features and the nonlinear decision functions that drive spiking in wing strain sensors. Since this paper is not yet online, it is included in this document as APPENDIX A. We also used micro-CT scanning to explore regions of the wing that contain patches of campaniform sensilla. Movies of these are available online as part of the supplemental material for that paper.
6. In Jankauski et al. (2017) we explored the novel concept that turning maneuvers in flapping flight animals (and vehicles) can arise from purely inertial dynamics of asymmetric wing strokes. Nearly all of the literature associated with turning control in flapping flight focuses solely on the aerodynamic forces that arise from asymmetric wing strokes. However, conservation of angular momentum suggests that such asymmetric flapping motions must necessarily require some net torque. Given that wing mass can be significant, we explored the possibility that wing inertia contributes to a significant part of the net torques resulting from asymmetric strokes. We developed a flapping wing model integrating aero and inertial dynamics. We showed that wing angular momentum varies with stroke deviation phase, implying a non-zero impulse during a time-dependent phase shift. Simulations show wing inertial and aerodynamic impulses are of similar magnitude during short transients, whereas aerodynamic impulses dominate during longer transients. Additionally, inertial effects become less significant for smaller flying insects. Thus, we conclude (a) modest changes in stroke deviation can significantly affect steering and (b) both aerodynamic and inertial torques are critical to maneuverability, the latter of which has not been considered. Since this paper is not yet online, it is included in this document as APPENDIX B.

In addition to these completed projects we have two more manuscripts nearing completion that owe their origins to research initiated on this grant. Since these are not available online, they are described below in a bit more detail than in the previously published papers.

1. With Thomas Mohren and Bing Brunton, we are completing a manuscript that extends our merger of sparse and compressive sensing methods with neural filters to explore optimal sensor placement for gyroscopic sensory functions associated with distributed strain sensors on wings. A key result is that a neural filter based on the stimulus features identified in Pratt et al. (2017), when combined with sparse sensor placement algorithms, greatly reduces the number of sensors needed to classify the effect of body rotation based on wing strain. Interestingly, without the neural filter, that classification is exceedingly difficult, even with 40 sensors

distributed over the wing. With that filter, as few as three sensors can accomplish this. We hope to submit this work to the Proceedings of the National Academy of Sciences within the next few months.

2. With Annika Eberle, Thomas Mohren, and Jessica Fox, we are finishing a manuscript that focuses on haltere strains. This was an offshoot of the work that showed how twisting motions arise in wings as a consequence of Coriolis forces acting on flapping and rotating wings. Interestingly, that twisting motion follows from how spatially distributed mass, when subject to Coriolis forces, experiences a torque that drives spanwise torsion. Prior computational work on halteres, however, treated them as point masses oscillating about some axis and subject to rotation about an orthogonal axis. Because of the point mass assumption, only lateral deflections can arise in response to Coriolis forces. However, if the end (knob) of the haltere is a distributed mass, the Coriolis force leads to a torsional deformation in addition to the lateral deflection predicted in prior literature. This mode of haltere deformation has not been reported in the literature and may profoundly affect our interpretation of strain sensing in halteres. We have built both computational (FEM) and analytic (Euler-Lagrange) models of haltere dynamics and demonstrated significant torsion. We are now using the stimulus features from Fox, Fairhall, and Daniel (2012) to predict the difference in campaniform spike responses that result from both torsion and lateral deflection. We hope to complete this manuscript within the next few months.

7 ABDOMINAL SENSING AND ACTUATION

Because of the critical importance of the wings, less attention has been paid to the role of body shape, or the “airframe,” of the animal for flight control. Changes in the shape of the body of an animal can alter the relative positions of the center of pressure on the body or its center of mass relative to the center of lift and thrust produced by wings. Thus, the body itself could be a key contributor to the system of actuators involved in flight control, exercising “airframe-based” control. Indeed, the control potential of body shape has been established for the passive, aerial descent paths of terrestrial lizards but not for flying animals. Over the course of this grant we sought to (1) characterize the mechanosensory structures in the abdomen of Manduca sexta and (2) establish extracellular recording techniques to characterize the encoding properties of abdominal proprioceptors.

In these past years we have accomplished a number of our goals regarding the role of sensorimotor dynamics of the airframe (abdomen) motion.

1. In Hinson et al. (2013) we showed that abdominal motions can be used for simultaneous actuation and state estimation (largely by a Coriolis sensing).
2. In Dyhr et al. (2013) we showed that abdominal flexion permits active control of the flight trajectory and allows movement right on the edge of stability.
3. In Cowan et al. (2014) we summarized the general topic of feedback control as a framework for understanding tradeoffs between stability and control. A portion of that study focused on airframe deformation as a control paradigm.

As with the wing strain sensing portion of this grant, we have additional ongoing projects on sensory information associated with abdominal position. To our knowledge no prior study has documented strain sensing in the abdomen in insect flight control, though we know it must be occurring. Adapting the experimental system that we established for wing strain sensing, we are now using multi-site extracellular electrode methods to more fully characterize the encoding properties of putative abdominal strain detectors. We are pleased to report that we have finally been able to record from the abdominal ventral nerve chord and use spike sorting algorithms along with multi-site electrodes to identify neurons that report abdominal motions. We presented that initial work in the 2015 meetings of the Society of Integrative and Comparative Biology (SICB) in Florida. A new paper on this topic was presented at the 2017 SICB meeting by Akriti Chadda.

Akriti Chadda, a visiting student from Hong Kong University of Science and Technology (HKUST), is co-advised by Professor Tom Daniel along with Professor I-Ming Hsing and Professor Wei Shyy of HKUST. She has been resident in the lab and has continued the efforts begun by earlier students focusing on the strain sensing and stimulus feature identification by mechanosensitive units extending from the abdomen into the ventral abdominal nerve chord of *Manduca*. She has identified a class of receptors that behave similarly to those found in wings, halteres, and even antennae: they all have similar stimulus features and similar nonlinear decision functions.

Jorge Bustamante, a new graduate student in the lab, has extended the work begun by Dyhr et al. (2012) to solve the full nonlinear system of differential equations that define flight control with a combination of both abdominal flexion (airframe deformation) and wing forces. He has developed a model-predictive controller (MPC) that uses a Monte-Carlo-based process to explore how complex flight paths can be controlled by airframe deformation. That work was initially presented at the 2017 SICB meetings, and a new version will be presented at the 2018 SICB meetings in San Francisco.

8 STUDENTS AND POSTDOCTORAL TRAINEES SUPPORTED BY THE GRANT

This list represents any form of salary support, even part time. Asterisks indicate an underrepresented minority or protected class.

Postdoctoral Trainees

Jonathan Dyhr is now Assistant Professor of Biology at Northwest University.

Eatai Roth is starting as Assistant Professor of Intelligent Systems Engineering at Indiana University.

Tanvi Deora is a recent recipient of the Human Frontiers of Science Program postdoctoral fellowship and continues to work in a research projected related to the grant.

Graduate and Post-baccalaureate Students

*Elischa Sanders** (Postbac) is now an MD/PhD Student in the UC San Diego Neuroscience program.

*Darrin Howell** (Postbac) is now a Research Scientist in the bio-motion lab at the University of Washington working with Dr. Sam Burden and Kat Steele.

*Brandon Pratt** (Postbac) is now a graduate student in the Quantitative Biology Program at Georgia Inst. Technology in the laboratory of Simon Sponberg.

*Octavio Campos** (Graduate student) has just completed his Ph.D. in Biology this summer and is seeking employment in the general area of recruiting and supporting under-represented minority students in the sciences.

Undergraduate Students

*Marissa Dominguez** (Biology Major at UW)

Nathan Berry (Biology Major at UW)

9 PEER-REVIEWED CONFERENCE PROCEEDINGS AND PUBLICATIONS ASSOCIATED WITH THIS PROJECT

1. Pratt, B., Deora, T., Mohren, T., and Daniel, T., “Neural Evidence Supports a Dual Sensory-Motor Role for Insect Wings,” *Proceedings of the Royal Society Biological Sciences*, (in press), 2017.
2. Jankauski, M., Daniel, T.L., and Shen, I.Y., “Asymmetries in Wing Inertial and Aerodynamic Torques Contribute to Steering in Insects,” *Bioinspiration & Biomimetics* (in press), 2017.
3. Roth, E., Hall, R.E., Daniel, T.L., and Sponberg, “The Integration of Parallel Mechanosensory and Visual Pathways Resolved through Sensory Conflict,” *Proceedings of the National Academy of Sciences of the United States of America,* pp. 12832–12837, doi: 10.1073/pnas.1522419113, 2016.
4. Sponberg, S., Dyhr, J., Hall, R., and Daniel, T.L., “Luminance Dependent Visual Processing Enables Moth Flight in Low Light,” *Science*, Vol. 348, pp. 1245–1248, June 12, 2015.
5. Brunton, B.W., Eberle, A., Dickerson, B., Brunton, S.L., Kutz, J.N., Daniel, T.L., “Sensor Placement and Enhanced Sparsity in a Sensory-Neural Decision,” *Computational and Systems Neuroscience (CoSyNe) Conference*, 2014.
6. Cowan, N.J., Ankarali, M.M., Dyhr, J.P., Madhav, M.S., Roth, E., Sefati, S., Sponberg, S., Stamper, S.A., Fortune, E.S., and Daniel, T.L., “Feedback Control as a Framework for Understanding Tradeoffs in Biology,” *Int. Comp. Biol.* (in press), 2014.
7. Dickerson, B., Aldworth, Z., Daniel, T., “The Control of Moth Flight Posture is Mediated by Wing Mechanosensory Feedback,” *Journal of Experimental Biology,* Vol. 217, pp. 2301-2308, doi: 10.1242/jeb.103770, 2014.
8. Dyhr, J.D., Morgansen, K.A., Daniel, T.L., and Cowan, N.J., “Flexible Strategies for Flight Control: An Active Role for the Abdomen,” *Journal of Experimental Biology*, Vol. 216, pp. 1523–1536, 2013.
9. Eberle, A.L., Reinhall, P.G., and Daniel, T. “Fluid-Structure Interaction in Compliant Insect Wings,” *Bioinspiration and Biomimetics,* Vol. 9, No. 2, doi: 10.1088/1748-3182/9/2/025005, 2014.
10. Eberle, A.L., Dickerson, B., Reinhall, P.G., and Daniel, T. “A New Twist on Gyroscopic Sensing: Body Rotations Lead to Torsion in Flapping, Flexing Insect Wings,” *Journal of the Royal Society Interface,* Vol. 12, No. 104, doi: 10.1098/rsif.2014.1088, 2015.
11. Hinson, B., Rombokas, E., Dyhr, J., Daniel, T., and Morgansen, K., “Sensing from Control: Airframe Deformation for Simultaneous Actuation and State Estimation,” *Control and Decision Conference*, Florence, 2013.

10 CONTRIBUTED PAPERS (NOT PEER-REVIEWED) FOR SCIENTIFIC MEETINGS ASSOCIATED WITH THIS PROJECT

1. Cowan, N.J., and Daniel, T.L., “Control and Dynamics of Movement in Biology: What Does Control Theory Have to Offer Integrative Biology?” *Soc. Integ. Comp. Biology*, Austin, TX, January 2014.
2. Dyhr, J.P., Sponberg, S., Hall, R., Colmenares, D.J., Chauhan, N.S., and Daniel, T.L., “Closing the Loop on Abdominal Control with Free Flight Pitch Perturbations,” *Soc. Integ. Comp. Biology*, Austin, TX, January 2014.
3. Dickerson, B.H., Sanders, E.J., Woods, J.I., and Daniel, T.L., “Multi-Channel Extracellular Recording Supports a Gyroscopic Function for Wings,” *Soc. Integ. Comp. Biology*, Austin, TX, January 2014.
4. Rombokas, E., Scheuer, L., Dyhr, J.P., and Daniel, T.L., “A Robotic Model of Inertial Flight Maneuvering in the Hawkmoth,” *Soc. Integ. Comp. Biology*, Austin, TX, January 2014.
5. Sanders, E., Woods, J., Dickerson, and Daniel, T.L., “Laser Localization of Wing Mechanosensory Cells with Multi-Site Recording,” *Integ. Comp. Biology*, West Palm Beach, FL, January 2015.
6. Howell, D., Woods, J., Chauhan, N., Sanders, E., Dyhr, J., and Daniel, T.L., “Insect Abdominal Mechanoreceptors Show Rapid Adaptation,” *Integ. Comp. Biology*, West Palm Beach, FL, January 2015.
7. Daniel, T.L., and Eberle, A., “*Unsteady Forces Form in Flapping Foils and Depend on Fluid-Solid Coupling in Water but not in Air*,” *Integ. Comp. Biology*, West Palm Beach, FL, January 2015.
8. Eberle, A., Dickerson, B., and Daniel, T.L., “Scaling of Gyroscopic and Aerodynamic Forces on Flapping Insect Wings during Body Rotations,” *Integ. Comp. Biology*, West Palm Beach, FL, January 2015.
9. Dickerson, B.H., Munk, Y., Roth, E., and Daniel, T.L., “Wing Mechanosensing Enhances Flight Responses to Visual Pitch,” *Integ. Comp. Biology*, West Palm Beach, FL, January 2015.
10. Daniel, T.L., “Sensing Actuators (or Actuating Sensors) in Flight Control,” *International Conference on Robotics and Actuation: Workshop on Robotics Inspired Biology*, Seattle, WA, May 2015.
11. Daniel, T.L., “Principles of Encoding,” *International Conference on Robotics and Actuation: Workshop on Animal Inspired Robust Flight*, Seattle, WA, May 2015.
12. Mohren, T.L., Eberle, A.L., Dickerson, B.H., and Daniel, T.L., “Gyroscopic Sensing by Flapping Wings: Strain Gauges Encode Body Angular Velocity,” *International Conference on Robotics and Actuation: Workshop on Robotics Inspired Biology*, Seattle, WA, May 2015.

13. “Identifying visual and mechanosensory pathways in a hawk moth flower-tracking behavior.” *International Conference on Robotics and Actuation: Workshop on Robotics Inspired Biology*, Seattle, May 2015.
14. Daniel T.L., “Sensing Actuators (or Actuating Sensors),” *International Congress of Robotics and Actuation*, Seattle, WA, 2015.
15. Mohren, T.L., Eberle, A.L., Dickerson, B.H., and Daniel, T.L., “Robotic Instantiation of Insect Wing Mechanoreception,” *International Congress of Robotics and Actuation*, Seattle, WA, 2015.
16. Roth, E., Hall, R.W., Daniel, T.L., Sponberg, S.N., “Identifying Visual and Mechanosensory Pathways in a Hawkmoth Flower Tracking Behavior,” *International Conference on Robotics and Actuation*. Seattle, WA, 2015.
17. Pratt, B.G., Dickerson, B.H., Sanders, E., Harris, M., Daniel, T.L., “Encoding Properties of Moth Wing Mechanoreceptors Are Similar to Haltere Neurons,” *Integ. Comp. Biology*, Portland, OR, January 2016.
18. Mohren, T.L, Dickerson, B.H., Pratt, B.G., Daniel, T.L., “Sensing Wing Deformation: It’s about Spike Time,” *Integ. Comp. Biology*, Portland, OR, January 2016.
19. Roth, E., Hall, R.W., Daniel, T.L., Sponberg, S.N., “Parallel Visual and Mechanosensory Pathways Mediate Flower-Tracking in the Hawkmoth Manduca sexta,” *Integ. Comp. Biology*, Portland, OR, January 2016.
20. Pratt, B.G., Mohren, T., Deora, T., Njonge, A., Daniel, T.L., “Focal Laser Energy Illuminates Strain Sensing in Insect Wings,” *Integ. Comp. Biology*, New Orleans, LA, January 2017.
21. Roth, E., Sponberg, S., and Daniel, T.L., “Robustness via Redundance: Multisensory Control of Flight in Hawkmoths,” *Integ. Comp. Biology*, New Orleans, LA, January 2017.
22. Mohren, T.L., Callaham, J., Pratt, B.G., Brunton, B., and Daniel, T.L., “Sparse Sensing by Arrays of Wing Mechanosensors for Insect Flight Control,” *Integ. Comp. Biology*, New Orleans, LA, January 2017.
23. Bustamante, J., Jankauski, M., and Daniel, T.L., “Wasp Waist: A Tail of Abdominal Flexion, Sensing, Actuation and Flight Control,” Integ. Comp. Biology, New Orleans, LA, January 2017.

APPENDIX A

ARTICLE IN PRESS

PROCEEDINGS B

rspb.royalsocietypublishing.org

Research

Cite this article: Pratt B, Deora T, Mohren T, Daniel T. 2017 Neural evidence supports a dual sensory-motor role for insect wings. *Proc. R. Soc. B* 20170969.
http://dx.doi.org/10.1098/rspb.2017.0969

Received: 3 May 2017
Accepted: 9 August 2017

Subject Category:
Morphology and biomechanics

Subject Areas:
biomechanics, neuroscience

Keywords:
flight control, campaniform sensilla, wings, strain sensing, Coriolis forces

Author for correspondence:
Thomas Daniel
e-mail: danielt@uw.edu

Electronic supplementary material is available online at rs.figshare.com.

THE ROYAL SOCIETY PUBLISHING

Neural evidence supports a dual sensory-motor role for insect wings

Brandon Pratt[1], Tanvi Deora[1], Thomas Mohren[2] and Thomas Daniel[1,2]

[1]Department of Biology, and [2]Department of Mechanical Engineering, University of Washington, Seattle, WA 98105, USA

TD, 0000-0002-5706-1096

Flying insects use feedback from various sensory modalities including vision and mechanosensation to navigate through their environment. The rapid speed of mechanosensory information acquisition and processing compensates for the slower processing times associated with vision, particularly under low light conditions. While halteres in dipteran species are well known to provide such information for flight control, less is understood about the mechanosensory roles of their evolutionary antecedent, wings. The features that wing mechanosensory neurons (campaniform sensilla) encode remains relatively unexplored. We hypothesized that the wing campaniform sensilla of the hawkmoth, *Manduca sexta*, rapidly and selectively extract mechanical stimulus features in a manner similar to halteres. We used electrophysiological and computational techniques to characterize the encoding properties of wing campaniform sensilla. To accomplish this, we developed a novel technique for localizing receptive fields using a focused IR laser that elicits changes in the neural activity of mechanoreceptors. We found that (i) most wing mechanosensors encoded mechanical stimulus features rapidly and precisely, (ii) they are selective for specific stimulus features, and (iii) there is diversity in the encoding properties of wing campaniform sensilla. We found that the encoding properties of wing campaniform sensilla are similar to those for haltere neurons. Therefore, it appears that the neural architecture that underlies the haltere sensory function is present in wings, which lends credence to the notion that wings themselves may serve a similar sensory function. Thus, wings may not only function as the primary actuator of the organism but also as sensors of the inertial dynamics of the animal.

1. Background

Animals rely on input from multiple sensory modalities to accomplish complex movement behaviours. From navigating in complicated habitats [1] to locating mates and avoiding prey [2,3], animals use visual, chemosensory, thermosensory and mechanosensory information to coordinate motor commands for the task at hand [4–8].

Animal flight control, in particular, strongly depends on multisensory integration due in part to the inherent instability associated with this mode of locomotion [9]. Unlike movement on land where multiple pairs of legs can provide stable support [10] or in water where instabilities have a vastly lower impact on movement control [11], flapping flight presents a stabilization challenge [9]. Whereas flight primarily relies on visual information, without which animals rarely fly, visual processing speeds are too slow to support rapid flight behaviours [12,13]. However, mechanosensory systems provide a rapid and parallel sensory processing pathway that compensates for slower visual systems [6,14–17].

In dipteran insects, halteres are thought to function as gyroscopic sensors that have the exquisite capacity to detect the Coriolis forces associated with body rotations [18–20]. By contrast, for the hawkmoth (*Manduca sexta*), a non-dipteran species that lacks halteres, Sane *et al.* [21] suggest that antennae also serve a similar

RSPB20170969—21/8/17—19:05–Copy Edited by: Not Mentioned

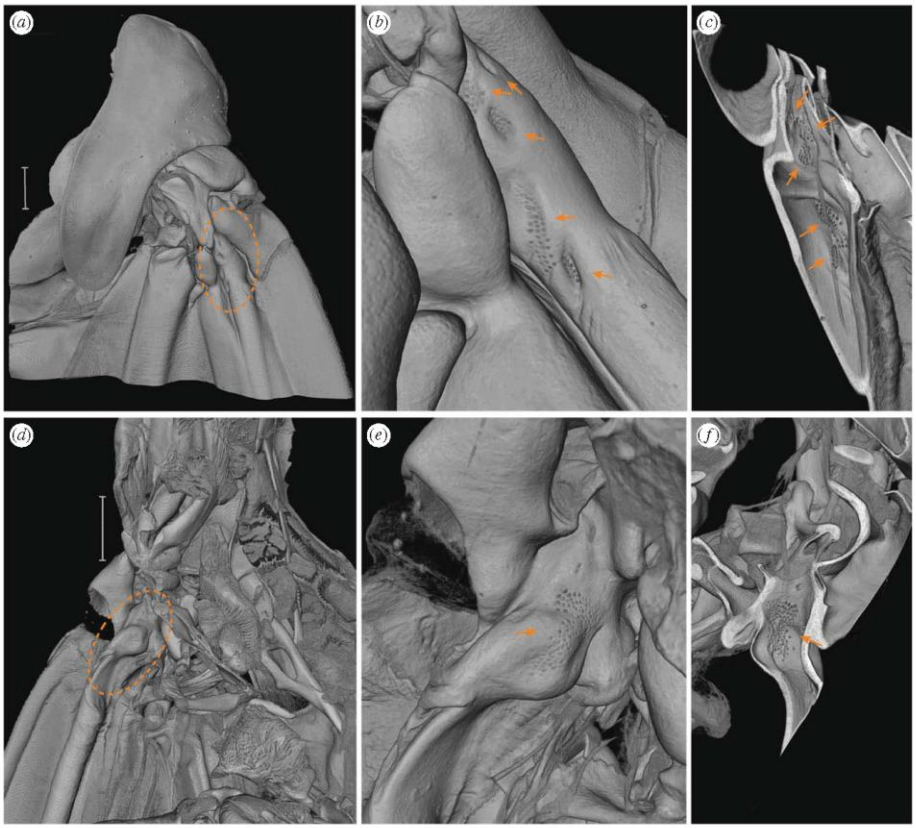

Figure 1. The wing surface contains multiple fields of campaniform sensilla. (*a*) Dorsal surface of the wing base with one sensilla-rich region highlighted (in dashed orange circle) and zoomed in (*b*,*c*). (*b*) Here, the campaniform sensilla occur in five distinct fields (orange arrows). (*c*) The same fields are visible from underneath, and can be viewed by virtually slicing the three-dimensional volume (orange arrows). (*d*) Ventral surface of the wing base with another sensilla field highlighted (in dashed orange circle) and zoomed in (*e*,*f*). (*e*) The highlighted sensilla field zoomed in and viewed on the ventral wing surface and (*f*) the ventral sensilla field is also visible by virtually slicing the three-dimensional volume to reveal it on a dorso-lateral view. (Online version in colour.) Q1

mechanosensory function [21]. In both cases, removal of halteres or antennae compromises flight performance [21,22]. Moreover, electrophysiological data from primary afferents associated with haltere mechanosensors (campaniform sensilla) show rapid and precise encoding of the forces acting on them [14–16]. There is similar evidence for the mechanosensory afferents of the moth antennae [23].

Halteres are evolutionarily derived from insect wings. For selection to act on wings in ways that could give rise to halteres, one would expect wings themselves to provide some level of information about Coriolis forces. Like halteres, wings contain numerous campaniform sensilla, some distributed over the surface of the wing and others arranged in patches near the base (figure 1, electronic supplementary material, movie S1) [24,25]. Biomechanical analyses showed that torsional deformations occur as a result of Coriolis forces acting on flapping wings during body rotations [26]. Moreover, recent behavioural evidence showed that in addition to visual information, hawkmoths use wing mechanosensory information to elicit postural changes associated with flight control [27].

With mounting evidence that wings themselves serve a sensory function similar to halteres, we asked if wings have the neural architecture in place to facilitate a gyroscopic function [28–30]. Here, we seek to characterize the encoding properties of wing campaniform sensilla to explore their similarity to haltere sensilla. Based on what is known about halteres [16], we hypothesize that (i) wing campaniform sensilla, like haltere neurons, encode mechanosensory information rapidly and precisely and (ii) there is a diversity in the encoding properties of the wing campaniform sensilla. Thus, in addition to the pure mechanosensory role ascribed to halteres, wings may serve the dual roles as both sensors and actuators.

2. Material and methods

(a) Animal preparation

All recordings were performed at 25°C (room temperature) on 1–3 days post-eclosion adult hawkmoths, *M. Sexta*, ($N = 33$, 16 males and 17 females) obtained from a colony maintained

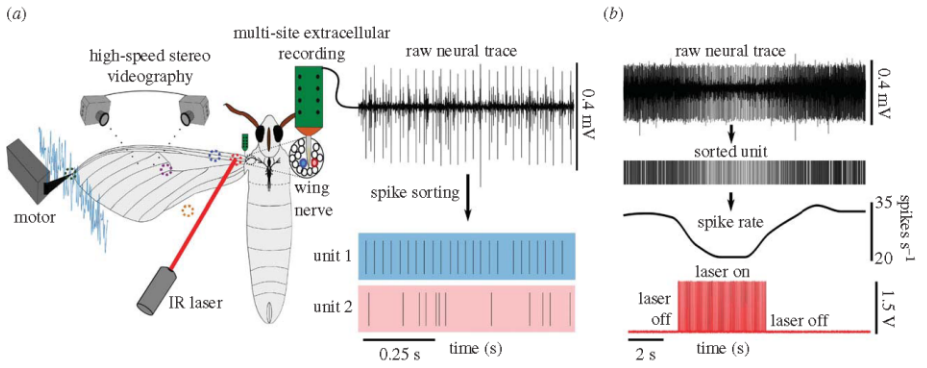

Figure 2. Experimental set-up for mechanically stimulating the wing campaniform sensilla in tandem with focal IR heating to identify their receptive fields on the wing surface and extract their encoding properties. (*a*) An anaesthetized moth was held in a custom-built immobilization chamber (not shown here) abducting the wing with the ventral surface facing up. A motor lever arm provided mechanical stimulus to the moth wing tip via a plastic grasp while we simultaneously recording the wing movements using two high-speed video cameras at 1000 fps allowing us to reconstruct wing displacement at specific locations on the wing. We used a multi-site extracellular electrode to record the resulting neural activity from the right forewing nerve (red trace). The extracellular neural data was spike sorted to reveal the activity of individual neuronal units (two sorted units shown in blue and red). Before applying the mechanical stimulus, we used focal IR laser heating at specific locations on the wing surface (dotted circles) while recording from the forewing nerve to reveal each neuronal unit's receptive field location on the wing. (*b*) A representative wing base-localized unit showing a reduction in firing rate (upper trace in black) during focal heating (lower trace in red). (Online version in colour.) Q1

at the University of Washington. Moths were collected in individual containers with a moist tissue to prevent desiccation. The moths were then anaesthetized at 4°C for approximately 24 h. They were prepared for recordings by removing the legs, the left-wing pair and the right hindwing. We descaled the cuticle around the base of the right forewing and painted white dots on the ventral wing surface using white acrylic paint. The dots were painted along the leading edge, the wing base and between the wing veins to be used as markers for reconstructing the time-varying changes in wing displacement arising from mechanical stimuli. Moths were anaesthetized at 4°C for another approximately 24 h before recording from the wing nerve. They were then placed in a custom designed three-dimensional printed immobilization holder such that the right forewing was abducted at approximately 90° from its normal resting position, with the ventral surface facing up for neural recordings (figure 2*a*). We exposed the right forewing nerve by removing the right tegula, basalare, and the trachea and other soft tissue overlying it. Two to three drops of physiological saline solution (150 mM NaCl, 3 mM $CaCl_2$, 3 mM KCl, 10 mM *N*-Tris [hydromethyl methyl]-2-aminoethanesulfonic acid buffer and 25 mM sucrose, pH 6.5–7.5) [31] were applied to the nerve as needed to prevent desiccation.

(b) Experimental procedure

(i) Electrophysiological recordings with simultaneous high-speed videography

We penetrated the right forewing nerve with a 16-channel extracellular electrode (model: A1 × 16-3 mm-25-177-A16, NeuroNexus, Ann Arbor, MI, USA). Neural signals were filtered and amplified (300–1000 Hz bandpass, 1000-fold amplification) using an extracellular amplifier (model 3600, A-M systems, Sequim, WA, USA) and recorded at 40 kHz using a data acquisition board (Model NI USB-6259, National Instruments, Austin, TX, USA). A tungsten wire, inserted through the cuticle on the lateral thorax, served as the reference electrode. In a typical preparation, we were able to maintain stable recordings of spiking activity in up to three simultaneous channels for more than 2 h.

We recorded the neuronal activity as we delivered mechanical stimuli to the wing tip through a motor lever arm (Model 305B, serial number 305034, Aurora Scientific Inc., Aurora, ON, Canada) via a plastic clasp. Custom MATLAB code (The Mathworks Inc., Natick, MA, USA) controlled the motor lever system to deliver three bouts of 25 Hz sinusoidal stimuli for 4 s, each of progressively larger wing tip amplitudes (peak to peak of 4.4, 8.8 and 13.2 mm, measured to the nearest 0.1 mm via an ocular micrometer). This was followed by 30 10-s bouts of band-limited (2–300 Hz) Gaussian white noise (hereafter white noise) of a maximum amplitude of 9.5 mm. There was a rest period of 1 s between the sinusoidal and the white noise segments, and a 2 s rest period between every 10 repeats of white noise stimuli. We sorted spikes to identify neuronal units using all channels that showed neural activity with NeuroExplorer® (V. 5, Nex Technologies, Madison, AL, USA) and Offline Sorter (V. 4, Plexon Inc., Dallas, TX, USA), using threshold and time alignment based on the spike peak, and sorted using PCA. The three axes of the PCA were based on two dominant principle components and the spike width. Spike time data were imported into MATLAB for further analyses. During the first 10-s presentation of the white noise mechanical stimulus, we recorded the three-dimensional position of wing markings using two high-speed video cameras (Miro-4M VR0308 and VR711, Vision research, Wayne, NJ, USA at 320 × 240 resolution, 1000 fps and 200–400 ms exposure) to compute wing region-specific mechanosensory stimuli (local displacements).

The high-speed videos of two male and two female wings were digitized and used to reconstruct the vertical displacement at their wing base (for an example of high-speed video and three-dimensional reconstruction (see electronic supplementary material, movie S2). The reconstruction was done using Tyson Hedrick's custom software in MATLAB [32]. We

used digitized data from these four moths to compute a transfer function (in gain and phase) relating displacements of the wing tip to wing base. We used this transfer function for units that were localized to the base (see below).

(ii) Laser-based focal heating to identify wing regions corresponding to campaniform receptive fields

Because all of the campaniform sensilla are mechanically coupled through the entire wing blade, using simple direct punctate mechanical stimuli make localizing the receptive fields quite challenging during electrophysiological recordings. To address this issue, we developed a new method to alter the activity of campaniform sensilla without the complication of stress localization. We relied on a combination of thermal sensitivity of campaniform sensilla [33–35] and a focused IR laser to localize regions of the wing. While simultaneously recording from the wing nerve using methods above, we focally heated specific locations on the wing surface with an IR laser (785 nm, 8 mW, model CDL-3144-008S laser diode, beam diameter of 0.5 mm, Sanyo, Japan). A custom-built Arduino circuit controlled the laser (figure 2*b*). Each location was heated five times at a duty factor of 25% for 5 s (100 pulses of 50 ms each). The duty factor was selected to provide a robust thermal response without damaging the wing. The input pulse to the laser was recoded along with the corresponding neural data on the data acquisition board at 40 kHz. Changes in the unit's firing rate during focal heating were used to localize the receptive field of that unit on the wing (see electronic supplementary material, figure S1 for details of how we classified thermally sensitive units).

(c) Computational analyses of the neuronal data

(i) Feature detection (spike-triggered averages and nonlinear decision functions)

We analysed only those identified units which had high stimulus-response coherence (high mutual information [36], for details of this process see electronic supplementary material). Using methods similar to previous studies [16,37], we computed the spike-triggered ensemble (STE) for each unit by selecting the stimulus history in the 40-ms time window immediately preceding each spike. Taking the mean of the STE yielded the spike-triggered average (STA). We also calculated the prior stimulus ensemble (PSE) by randomly selecting time stamps throughout the white noise stimulus period, and similarly selecting the 40-ms stimulus history preceding each of those timestamps. The total number of timestamps for the generating the PSE was the same as the recorded number of spikes for each unit.

To characterize the nonlinear decision function (NLD), we computed a histogram of the projections of the STA onto the stimulus for each spike (each element of the STE) with a bin width of 0.4 of the standard deviation of the PSE. We normalized this histogram by dividing each bin by the product of the norm of the STA and each element of the STE. Similarly, we constructed and normalized a histogram of the projections of the STA onto each element of the PSE. We then constructed the NLD histogram by dividing the normalized histogram built from the STE by the normalized histogram built from the PSE. This histogram was converted into predicted spike rate by multiplying it by the mean firing rate of the unit during the white noise stimulus period. We then performed a cubic spline interpolation between the predicted spike rates of each bin to fit a curve onto this histogram.

Normalizing in this manner ensured that the NLD had a value between −1 and 1. The NLD represents the selectivity of a unit in response to any particular stimulus.

(ii) One-dimensional spike rate prediction model

Using the STA and NLD of a unit, we predicted its spike rate in response to the three different amplitudes (4.4, 8.8 and 13.2 mm) of sinusoidal stimuli. We convolved the STA with the 40 ms cycle of the sinusoidal stimuli and normalized the projection value in a similar manner to the NLD construction. For each projection value, we used the NLD to calculate the corresponding predicted spike rate. We compared the predicted spike rate with the recorded spike rate by reconstructing a recorded spike rate histograms. This recorded spike rate histogram was built by binning over a 1.25 ms time window and averaging the spike rate across the 100 repeats of a single 40 ms sinusoidal cycle. To compensate for binning artefact, we further convolved the histogram with a 40 ms Gaussian window ($\sigma = 5.3$ ms). We calculated the root-mean-square error between the predicted spike rate and the fitted recorded spike rate as a measure of how well the one-dimensional spike rate prediction model predicts a unit's spike rate during the sinusoidal stimuli.

3. Results

We acquired multi-channel extracellular recordings of the wing afferents from a total of 33 hawkmoths, *M. sexta*, while delivering mechanical stimuli to the wing tip. We identified 95 wing mechanosensory units using offline spike sorting techniques (figure 2*a*; *Methods and materials*). To study the encoding properties of these campaniform sensilla, it was essential to approximate the local mechanical stimulus experienced by each sensillum during perturbations to the wing tip. Hence we drew upon the thermosensitive properties of mechanosensors and developed a novel laser-based focal heating method to localize the receptive field of each afferent. We captured high-speed videos (1000 fps) of the wing during mechanical stimulation to reconstruct the local displacements at different regions on the wing.

(a) Focal heating reveals local displacements for identified receptive fields

Focal heating combined with multi-channel extracellular recording and high-speed videography allowed us to reconstruct the local displacements for identified receptive fields. In our experiments, most units showed a reduction in firing rate when heated (figure 2*b*) although a small subset of units showed an increase. This focal heating technique allowed us to localize 31 units to the wing base (for details see electronic supplementary material, figure S1 and methods). The remaining 64 units could not be localized to any region on the wing. Most of these units were not tonically active and hence we could not observe changes in firing rate during local heating. We cannot rule out the possibility that the non-localized units also project from the wing base. We used the reconstructed wing displacement associated with the 31 units localized to the wing base (referred to as the *base-localized*

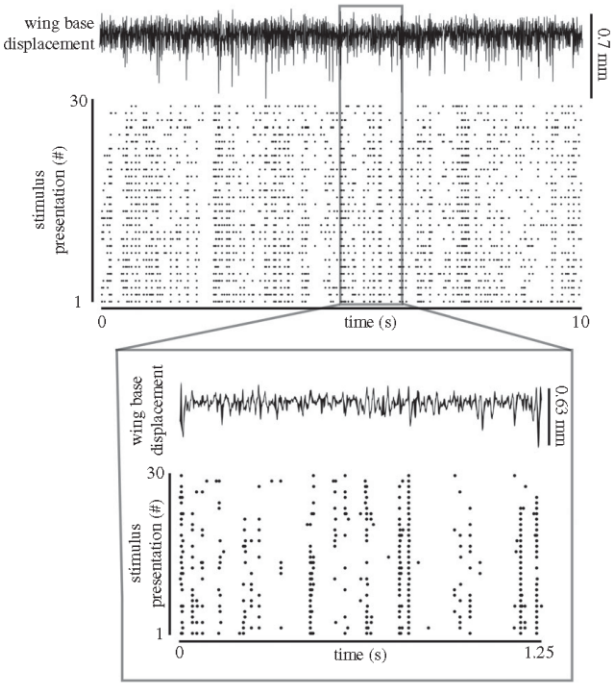

Figure 3. Forewing mechanosensory units fire reliably to repeated white noise mechanical stimuli. Raster plot showing the spike timing for a representative mechanosensory unit projecting from the wing base (*lower plot*; each dot represents a single spiking event) in response to repeated 10-s-long, band-limited (2–300 Hz) white noise mechanical stimuli delivered to the wing tip. Vertical displacement at the wing base estimated from high-speed stereo videography (*upper trace*).

units), and the wing tip deflection for the other 64 units (referred to as the *non-localized units*) for further analyses.

From our calculations for the signal response (SR) coherence between the spike train of each unit and the motion stimulus (see electronic supplementary material for details on SR coherence analysis, figure S2), 14 out of the 31 base-localized mechanosensory units and 34 of the 64 non-localized mechanosensory units had a significant SR coherence at one or more frequencies (SR coherence of the unit's spike train and mechanical stimulus greater than 95% CI of a distribution of SR coherence of randomly permuted spike train and mechanical stimulus). These 14 base-localized and 34 non-localized units were used for further analyses using either the base or wing tip deflection as estimates of the mechanical stimulus driving their activity.

(b) Wing mechanosensory units show rapid and selective encoding for a diversity of features

To identify how wing campaniform sensilla encode mechanical stimuli, we analysed the response to 10 repeats of 10-s-long, band-limited (2–300 Hz) white noise mechanical stimulus. The consistency of the units' spike timing during the 30 white noise repeats (figure 3) suggests strong stimulus feature selectivity. We used the STA to compute the feature of wing displacement driving neural activation. Different units have varying STA shapes indicating diversity in the encoding properties of wing campaniform sensilla (figure 4*a*(i)(ii),*b*(i)(ii); base-localized units, figure 4*c*(i)(ii),*d*(i)(ii); non-localized units). The amplitude of the base-localized unit's STA reveals that these units respond to stimuli at least as small as 0.15 mm (figure 4*a*(i),*b*(i)). To determine how rapidly these units encode mechanical information, we measured the mean time at which the STA reached its maximum absolute value displacement from rest. The latency of firing (shown as means $\pm$ s.d.) for the base-localized units was 1.9 ± 2.1 mss ($n = 14$) and 2.8 ± 1.8 ms ($n = 34$) for the non-localized units. Another measure for latency is the time at which the standard deviation of the STA is at its minimum. This latter metric indicates the time prior to a stimulus when the motion amplitude and its time history most reliably lead to a response. Both are fairly similar measures of the timing relative to a spike. Using this measure, the latency for the base-localized units was 10.6 ± 10.5 ms ($n = 14$) and 5.1 ± 1.6 ms for the non-localized units ($n = 34$). Thus, the mechanosensory units showed low latency spike timing to specific features of the wing displacement.

We examined all of the STAs using singular value decomposition (SVD), which, like a PCA, extracts the dominant characteristics of the stimulus waveforms that initiate spikes (see electronic supplementary material for details and methods on the SVD analysis, figures S3 and S4). Two dominant modes weighted for their singular values show similar shapes with similar latencies and contain most of the energy of stimulus features that drive responses. The

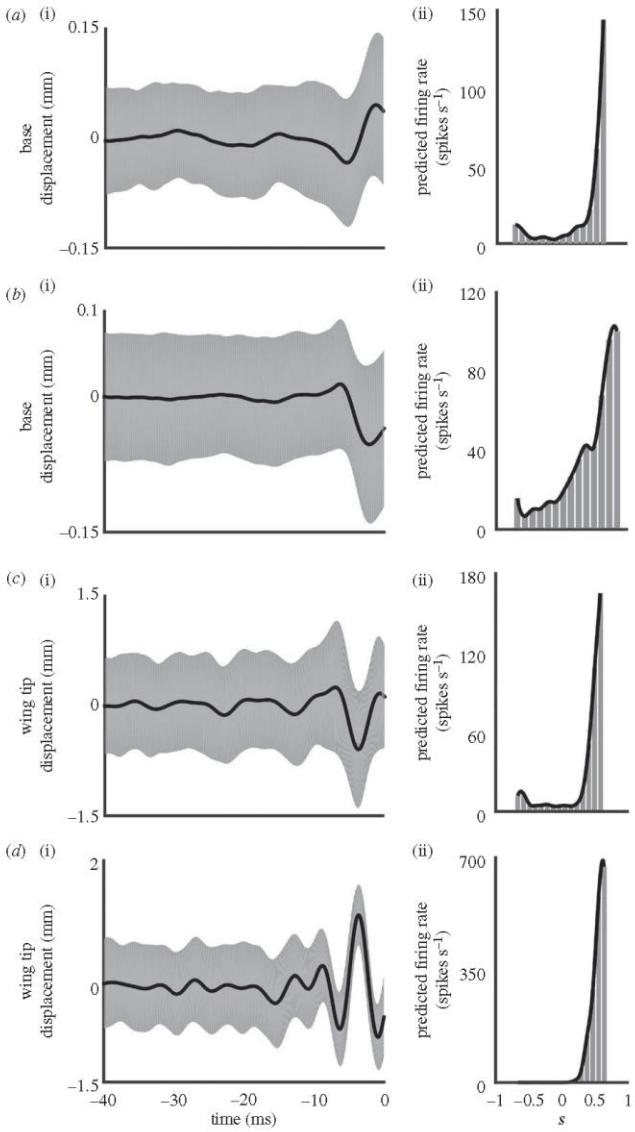

Figure 4. Wing mechanosensory units respond rapidly and selectively to diverse stimulus features as shown by their STAs and nonlinear decision functions (NLDs). STAs (*a*(i),*b*(i),*c*(i),*d*(i) STA in black ± s.d. in light grey) for two representative wing mechanosensory units projecting from the wing base (*a*,*b*) and two representative units not localized to a region on the wing (*c*,*d*) are plotted for the 40 ms prior to spike occurrences. These units show that stimulus motions within 10 ms yield spikes. The NLDs (*a*(ii),*b*(ii),*c*(ii),*d*(ii) grey histogram of the predicted spike rate over a range of stimulus projections and the fitted curve in black) for each of the representative mechanosensory units is plotted as the predicted firing as a function of the similarity of the stimulus to the STA. That similarity (***s***) is computed by the projection STA onto the stimulus and was normalized to their respective amplitudes. The sharp rise in the NLD as the ***s*** tends to 1 shows that the unit is highly selective for stimulus features that resemble the STA.

second mode resembles the derivative of the first dominant mode. In general, all STAs show similar latencies to that of the dominant modes.

We constructed the one-dimensional NLDs of these units as a measure of their selectivity for particular stimulus features (figure 4*a*(ii),*b*(ii), *c*(ii),*d*(ii)). The shape of the NLD is a measure of the unit's selectivity. We characterized the selectivity of identified units by calculating the value of the normalized stimulus projection at half of the maximum predicted spike rate: more selective units have a higher value for the projected

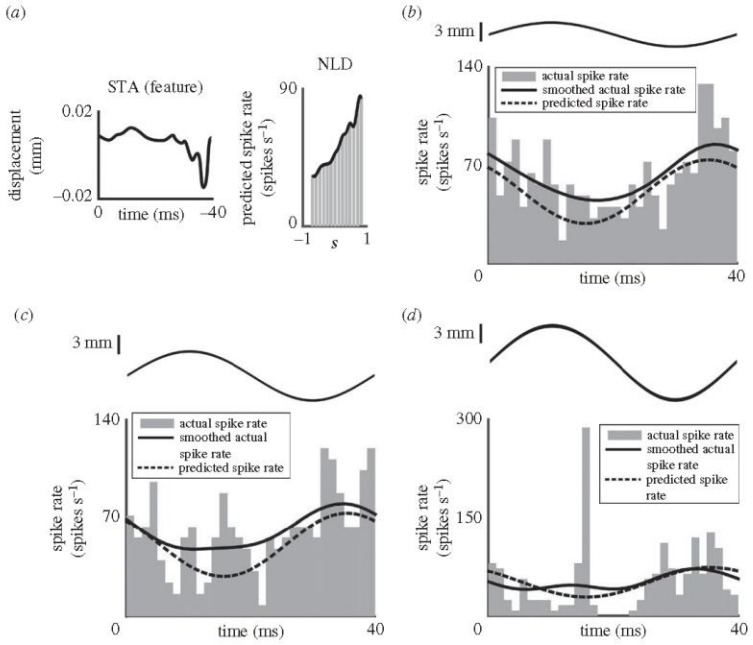

Figure 5. The one-dimensional spike rate prediction model extracted from the white noise mechanical stimulus captures the response of wing mechanosensory units to a novel sinusoidal stimuli. (*a*) The STA and NLD for a representative wing base unit were used to predict its spike rate in response to a 25 Hz sinusoidal wing displacement of varying amplitudes (*b*) 4.4 mm; (*c*) 8.8 mm and (*d*) 13.2 mm, black lines above each panel. The predicted spike rate (the black dashed line) closely resembles the recorded spike rate (black line). The recorded spike rate histogram in represented by grey bars. The predicted spike rates match measured spike rates more reliably at lower amplitudes. We used 100 repeats of sinusoidal mechanical stimuli at each amplitude to reconstruct the average recorded spike rate.

half maximum. The normalized projection value at half maximum was 0.18 ± 0.45 for the base-localized units (mean $\pm$ s.d., $n = 14$) and 0.44 ± 0.12 for the non-localized units (mean $\pm$ s.d., $n = 34$). Comparing these to the stimulus projection value at the largest predicted firing rate (0.59 ± 0.36 for the 14 base-localized units and 0.59 ± 0.09 for the 34 non-localized units) shows strong selectivity.

(c) The one-dimensional spike rate model constructed from white noise stimuli predicts a unit's spike rate to novel sinusoidal stimuli

We predicted the response of a unit to 25 Hz sinusoidal stimuli using the STA and NLD constructed from the white noise mechanical stimuli (figure 5 and for raw neural activity during the sinusoidal displacement, see electronic supplementary material, figure S5). The predicted spike rate (black dashed line) captures the shape of the smoothed recorded spike rate (solid black line) for a representative unit over one sinusoidal cycle (average spike rate histogram binned over 1.25 ms across 100 repeats; in grey). This spike rate prediction model faithfully predicts the unit's recorded spike rate during sinusoidal displacements as shown by a relatively small root mean square error between the predicted and recorded spike rates (see electronic supplementary material, figure S6 and table S1). The smaller amplitude sine wave corresponds to the energy present at that frequency in the white noise stimulus used to extract the STA. That lower amplitude sine stimulus shows closer agreement between measurement and prediction than is the case for higher amplitude stimuli. All three amplitudes show a peak of spike activity shortly following the minimum displacement. At higher amplitudes (figure 5*c*,*d*) spike activity appears at a time shortly after the maximum displacement of the sine stimulus.

4. Discussion and conclusion

Four key findings emerged from this study. First, the primary afferents projecting from campaniform sensilla, both those localized at the wing base and those that could not be localized, showed rapid responses to mechanical stimuli, often within approximately 2 or 3 ms. Second, there is variation in the shape of the stimulus features (STA) that drive responses. Third, the shapes of the NLD indicate strong selectivity for particular stimulus features. Fourth, using the STAs and NLDs of the wing mechanosensory units, we were able to predict the empirical spike rates during sinusoidal displacements of varying amplitudes to the wing. These results provide strong neural evidence for the similarity in the encoding properties between wing and haltere mechanosensory neurons. Indeed, nearly all of these results recapitulate those found by *Fox et al.* [16] for haltere neurons, which also encode mechanosensory information rapidly and precisely. In that study, 36 recorded haltere neurons responded in 3.0 ± 2.8 ms to specific stimulus features

[15,16], and therefore, had rapid and precise spike timing. This corresponds with our results from wing mechanosensory neurons. Haltere neurons also demonstrated variability in their encoding properties in regards to the shape of their STAs [16] in ways that strongly resemble the variation we note for wing campaniform sensilla. Haltere neurons were further found to be highly selective for particular stimulus features as indicated by their NLDs [16]. Collectively these similarities suggest that the neural equipment encoding mechanosensory information is common to both wings and halteres. Therefore, like halteres, wings may serve a similar sensory function [18]. Most importantly, these data support the ideas raised by Eberle *et al.* [26] and Dickerson *et al.* [27] that wings may serve a role as sensors of body dynamics.

While we have strong evidence for this dual actuator and sensor role for wings, our estimates of the strain experienced by any one campaniform sensillum require technology with vastly higher spatial and temporal precision than afforded by our current methods involving multi-camera high-speed videography and three-dimensional reconstruction. For the 34 units that we could not spatially localize on the wing, we used the vertical displacement of the wing tip as a proxy for the strains that these sensilla experienced during mechanical perturbations to the wing. Prior studies of haltere neurons were also limited in their inability to reconstruct the precise stimuli experienced by a single sensillum [16]. Insect wings are composed of a complex matrix of rigid veins that provide stiffness to the wing and thin cuticular sheets that are flexible and folded into various complex shapes. Any motion delivered to the wing tip is filtered by the wing's shape and spatial stiffness distribution such that local regions on the wing surface might experience different strains; altered both in phase and amplitude (see electronic supplementary material, movie S2) [26,38,39]. Knowing the strain at the level of a single campaniform sensillum will reveal a more proximate estimate of the feature detection for these sensors, and a potentially better understanding of the variation found among their encoding properties [40]. An important caveat is that precise calculation of strain requires equally precise information about details of the cuticular structures surrounding and including each sensillum. Thus we believe larger scale estimates of mechanical stimuli are sufficient. Moreover, our ability to use measured STAs and NLDs to reconstruct observed neural responses lends credence to this approach.

Drawing on the thermosensitive properties of campaniform sensilla permitted a novel method for localizing receptive fields in an extracellular recording preparation. However, a second limitation in this work is that only tonically firing units could be localized. Thus, we examine a subset of the possible units that may contribute to wing sensing. Nevertheless, the subset of units shows sufficient similarity to the range and quality of responses found in haltere neurons to justify this approach.

Because we used extracellular recording techniques, we can never be 100% certain that spikes that are sorted and clustered correspond to a particular neuron (campaniform sensillum). For intracellular recording, we would be far more confident, as was the case for Fox *et al.* [16], that the recorded spikes were form a single neuron. As it is, we used two leading principal components (including timing coincidence on multiple channels, and spike width) and the peak-to-valley amplitude. While this is a stricter classification process than one using equivalent spike amplitudes, there is a remote possibility that more than one sensillum responded at the same time with the same spike shape. Additionally, we used a fairly stringent test to select only those units whose signal to response coherences was, via bootstrap methods, statistically significant. This metric, together with our spike sorting algorithms, makes us fairly confident that we are dealing with single campaniforms.

As mentioned above, the STA and NLD derived from a white noise stimulus was used to predict spike responses to the more physiologically relevant mechanical stimulus of a 25 Hz sine stimulus (figure 5). That prediction, however, was less effective at stimulus amplitudes that were higher than those associated with the white noise stimulus. Our ability to deliver larger amplitude white noise stimuli was limited by the total energy we could impart to the wing without incurring significant damage, likely a consequence of the energy at the higher frequencies. That said, the relationship between predicted and measured spike rate was fairly robust for the spiking associated with the peak downward (minimum) wing deflection stimulus. At the peak upward stimulus the unit activity, initially relatively modest at low amplitudes, begins to appear at larger amplitudes. This may be a consequence of a feature of insect mechanoreceptors that demonstrate responses to both stimulus onset and offset (e.g. [40]).

Despite these limitations, prior work [26,27] and our current results provide strong evidence that wings could serve a function in sensing inertial dynamics of the body. Indeed, because halteres are derived from wings, evolution suggests that the function of gyroscopic sensing in halteres was likely present in such ancestral structures. Eberle *et al.* [26] previously demonstrated that the torsion arising when a flapping and flexing wing experiences rotational forces could lead to changes in the pattern of strain over the surface of the wing. They further suggested that torsion would influence the spatial and temporal pattern of neural activity of wing campaniform sensilla. Additionally, behavioural results from Dickerson *et al.* [27] showed that mechanical stimulation to wings drove stabilization reflexes. Together, the results from Eberle *et al.* [26] and Dickerson *et al.* [27] support the idea that wings function as sensors of body dynamics. Here, we add additional support to this idea by highlighting the similarities in the encoding properties of wing and haltere campaniform sensilla [16].

There is still more to understand at the circuit level about how mechanosensory information is processed, integrated, and transformed into behavioural outputs [40,41]. It may be that similar research on a range of taxa can reveal common encoding properties and possible functions of wing campaniform sensilla, especially given the immense diversity in wing morphology across all insect taxa [38]. Additionally, how campaniform sensilla are distributed over the wing blade and how that distribution varies taxonomically remains an open issue [24,42]. Indeed, recent studies of optimal sensor placement in a few taxa show that flapping dynamics are best detected with concentrations of campaniforms at the base [43]. However, more complex dynamics, such as body rotations or accelerations in various axes will drive even more complex wing deformations. Those deformations, filtered through the neural responses of a distribution of sensors, could be used to classify or measure body rotations and accelerations about multiple axes.

Ethics. No vertebrate animals were used in this research. Moths were cold anaesthetized prior to preparation for neural recordings.

Data, code and materials. All data are uploaded into the Dryad system: http://dx.doi.org/10.5061/dryad.7hm1m [44]. Code is available on Github at https://github.com/Prattbuw/CODE-Neural-evidence-supports-a-dual-sensory-motor-role-for-insect-wings-Pratt-et-al.

Authors' contributions. B.P. and T.D. carried out all experiments. B.P., T.D., T.M. and T.L.D. were involved in data analysis and paper writing. T.D. carried out all micro-CT imaging. T.L.D. conceived of the study. All authors gave their final approval.

Competing interests. We declare we have no competing interests.

Funding. This work was funded by the AFRL grant (FA8651-12-1004), AFSOR grant nos. (FA9550-14-1-0398 and FA9550-11-1-0155), Komen Endowed Chair, Washington Research Foundation Funds for Innovations in Neuroengineering awarded to Tom Daniel, the Washington Research Foundation Innovation Graduate Fellowship in Neuroengineering to Thomas Mohren, and the Washington Research Foundation Innovation Undergraduate Fellowship in Neuroengineering and the Mary Gates Research Scholarship awarded to Brandon Pratt.

Acknowledgements. We thank Arianna Njonge, Monica Harris, Darren Howell, Elisha Sanders, Jared Callaham and Brad Dickerson for their help in setting up this project, and for collecting and analysing data. We also thank Katie Stanchak for help with micro-CT imaging and Wai Pang Chan for preparation of micro-CT samples. The imaging and analysis of these samples were performed in Sharlene Santana and Christian Sidor's Labs at the University of Washington. We also thank the Riffell, Brunton and Fox Labs for their contribution to this work.

References

1. Arleo A, Rondi-Reig L. 2007 Multimodal sensory integration and concurrent navigation strategies for spatial cognition in real and artificial organisms. *J. Integr. Neurosci.* **6**, 327–366. (doi:10.1142/S0219635207001593)
2. Edwards DH, Heitler WJ, Krasne FB. 1999 Fifty years of a command neuron: the neurobiology of escape behavior in the crayfish. *Trends Neurosci.* **22**, 153–161. (doi:10.1016/S0166-2236(98)01340-X)
3. Land M, Collett T. 1974 Chasing behaviour of houseflies (*Fannia canicularis*). *J. Comp. Physiol.* **89**, 331–357. (doi:10.1007/BF00695351)
4. Taylor GK, Krapp HG. 2007 Sensory systems and flight stability: what do insects measure and why? *Adv. Insect Phys.* **34**, 231–316. (doi:10.1016/S0065-2806(07)34005-8)
5. van Breugel F, Riffell J, Fairhall A, Dickinson MH. 2015 Mosquitoes use vision to associate odor plumes with thermal targets. *Curr. Biol.* **25**, 2123–2129. (doi:10.1016/j.cub.2015.06.046)
6. Bender JA, Dickinson MH. 2006 Comparison of visual and haltere-mediated feedback in the control of body saccades in *Drosophila melanogaster*. *J. Exp. Biol.* **209**, 4597–4606. (doi:10.1242/jeb.02583)
7. Sherman A, Dickinson MH. 2003 A comparison of visual and haltere-mediated equilibrium reflexes in the fruit fly *Drosophila melanogaster*. *J. Exp. Biol.* **206**, 295–302. (doi:10.1242/jeb.00075)
8. Raguso RA, Willis MA. 2005 Synergy between visual and olfactory cues in nectar feeding by wild hawkmoths, *Manduca sexta*. *Anim. Behav.* **69**, 407–418. (doi:10.1016/j.anbehav.2004.04.015)
9. Hedrick TL, Daniel TL. 2006 Flight control in the hawkmoth *Manduca sexta*: the inverse problem of hovering. *J. Exp. Biol.* **209**, 3114–3130. (doi:10.1242/jeb.02363)
10. Full RJ. 2002 Quantifying dynamic stability and maneuverability in legged locomotion. *Integr. Comp. Biol.* **42**, 149–157. (doi:10.1093/icb/42.1.149)
11. Weihs D. 2002 Stability versus maneuverability in aquatic locomotion 1. *Integr. Comp. Biol.* **42**, 127–134. (doi:10.1093/icb/42.1.127)
12. Theobald JC, Warrant EJ, O'Carroll DC. 2010 Wide-field motion tuning in nocturnal hawkmoths. *Proc. Biol. Sci.* **277**, 853–860. (doi:10.1098/rspb.2009.1677)
13. Sponberg S, Dyhr JP, Hall RW, Daniel TL. 2015 Luminance-dependent visual processing enables moth flight in low light. *Science* **348**, 1245–1248. (doi:10.1126/science.aaa3042)
14. Fayyazuddin A, Dickinson MH. 1996 Haltere afferents provide direct, electrotonic input to a steering motor neuron in the blowfly, *Calliphora*. *J. Neurosci.* **16**, 5225–5232.
15. Fox JL, Daniel TL. 2008 A neural basis for gyroscopic force measurement in the halteres of Holorusia. *J. Comp. Physiol. A* **194**, 887–897. (doi:10.1007/s00359-008-0361-z)
16. Fox JL, Fairhall AL, Daniel TL. 2010 Encoding properties of haltere neurons enable motion feature detection in a biological gyroscope. *Proc. Natl Acad. Sci. USA* **107**, 3840–3845. (doi:10.1073/pnas.0912548107)
17. Roth E, Hall RW, Daniel TL, Sponberg S. 2016 Integration of parallel mechanosensory and visual pathways resolved through sensory conflict. *Proc. Natl Acad. Sci. USA* **113**, 12 832–12 837. (doi:10.1073/pnas.1522419113)
18. Pringle JWS. 1948 The gyroscopic mechanism of the halteres of *Diptera*. *Phil. Trans. R. Soc. Lond. B* **233**, 347–384. (doi:10.1098/rstb.1948.0007)
19. Yarger AM, Fox JL. 2016 Dipteran halteres: perspectives on function and integration for a unique sensory organ. *Integr. Comp. Biol.* **56**, 865–876. (doi:10.1093/icb/icw086)
20. Nalbach G, Hengstenberg R. 1994 The halteres of the blowfly Calliphora II. Three-dimensional organization of compensatory reactions to real and simulated rotations. *J. Comp. Physiol.* **175**, 695–708.
21. Sane SP, Dieudonné A, Willis MA, Daniel TL. 2007 Flight control in moths. *Science* **315**, 863–866. (doi:10.1126/science.1133598)
22. Dickinson MH. 1999 Haltere-mediated equilibrium reflexes of the fruit fly, *Drosophila melanogaster*. *Phil. Trans. R. Soc. Lond. B* **354**, 903–916. (doi:10.1098/rstb.1999.0442)
23. Dieudonné A, Daniel TL, Sane SP. 2014 Encoding properties of the mechanosensory neurons in the Johnston's organ of the hawk moth, *Manduca sexta*. *J. Exp. Biol.* **217**, 3045–3056. (doi:10.1242/jeb.101568)
24. Cole ES, Palka J. 1982 The pattern of campaniform sensilla on the wing and haltere of *Drosophila melanogaster* and several of its homeotic mutants. *J. Embryol. Exp. Morphol.* **71**, 41–61.
25. Agrawal S, Grimaldi D, Fox JL. 2017 Haltere morphology and campaniform sensilla arrangement across *Diptera*. *Arthropod Struct. Dev.* **46**, 215–229. (doi:10.1016/j.asd.2017.01.005)
26. Eberle AL, Dickerson BH, Reinhall PG, Daniel TL. 2015 A new twist on gyroscopic sensing: body rotations lead to torsion in flapping, flexing insect wings. *J. R. Soc. Interface* **12**, 20141088. (doi:10.1098/rsif.2014.1088)
27. Dickerson BH, Aldworth ZN, Daniel TL. 2014 Control of moth flight posture is mediated by wing mechanosensory feedback. *J. Exp. Biol.* **217**, 2301–2308. (doi:10.1242/jeb.103770)
28. Gettrup E. 1965 Sensory mechanisms in locomotion: the campaniform sensilla of the insect wing and their function during flight. *Cold Spring Harb. Symp. Quant. Biol.* **30**, 615–622. (doi:10.1101/SQB.1965.030.01.059)
29. Dickinson MH. 1990 Comparison of encoding properties of campaniform sensilla on the fly wing. *J. Exp. Biol.* **151**, 245–261.
30. Bartussek J, Lehmann F-O. 2016 Proprioceptive feedback determines visuomotor gain in *Drosophila*. *R. Soc. open Sci.* **3**, 150562. (doi:10.1098/rsos.150562)
31. Lei H, Christensen TA, Hildebrand JG. 2004 Spatial and temporal organization of ensemble representations for different odor classes in the moth antennal lobe. *J. Neurosci.* **24**, 11 108–11 119. (doi:10.1523/JNEUROSCI.3677-04.2004)
32. Hedrick TL. 2008 Software techniques for two- and three-dimensional kinematic measurements of biological and biomimetic systems. *Bioinspir. Biomim.* **3**, 34001. (doi:10.1088/1748-3182/3/3/034001)
33. Gingl E, Hinterwirth A, Tichy H. 2005 Sensory representation of temperature in mosquito warm and cold cells. *J. Neurophysiol.* **94**, 176–185. (doi:10.1152/jn.01164.2004)
34. Must A, Merivee E, Mand M, Luik A, Heidemaa M. 2006 Electrophysiological responses of the antennal campaniform sensilla to rapid changes of temperature in the ground beetles *Pterostichus oblongopunctatus* and *Poecilus cupreus* (Tribe Pterostichini) with different ecological preferences. *Physiol. Entomol.* **31**, 278–285. (doi:10.1111/j.1365-3032.2006.00518.x)

35. Clapham DE. 2003 TRP channels as cellular sensors. *Nature* **426**, 517–524. (doi:10.1038/nature02196)
36. Borst A, Theunissen FE. 1999 Information theory and neural coding. *Nat. Neurosci.* **2**, 947–957. (doi:10.1038/14731)
37. Aljadeff J, Lansdell BJ, Fairhall AL, Kleinfeld D. 2016 Analysis of neuronal spike trains, deconstructed. *Neuron* **91**, 221–259. (doi:10.1016/j.neuron.2016.05.039)
38. Combes SA, Daniel TLD. 2003 Flexural stiffness in insect wings I. Scaling and the influence of wing venation. *J. Exp. Biol.* **206**, 2979–2987. (doi:10.1242/jeb.00523)
39. Combes SA, Daniel TLD. 2003 Flexural stiffness in insect wings II. Spatial distribution and dynamic wing bending. *J. Exp. Biol.* **206**, 2989–2997. (doi:10.1242/jeb.00524)
40. Dickinson MH, Palka J. 1987 Physiological properties, time of development, and central projection are correlated in the wing mechanoreceptors of *Drosophila*. *J. Neurosci.* **7**, 4201–4208.
41. Ando N, Wang H, Shirai K, Kiguchi K, Kanzaki R. 2011 Central projections of the wing afferents in the hawkmoth, *Agrius convolvuli*. *J. Insect Physiol.* **57**, 1518–1536. (doi:10.1016/j.jinsphys.2011.08.002)
42. Ray RP, Nakata T, Henningsson P, Bomphrey RJ. 2016 Enhanced flight performance by genetic manipulation of wing shape in *Drosophila*. *Nat. Commun.* **7**, 10851. (doi:10.1038/ncomms10851)
43. Hinson BT, Morgansen KA. 2015 Gyroscopic sensing in the wings of the hawkmoth *Manduca sexta*: the role of sensor location and directional sensitivity. *Bioinspir. Biomim.* **10**, 56013. (doi:10.1088/1748-3190/10/5/056013)
44. Pratt B, Deora T, Mohren T, Daniel T. 2017 Data from: Neural evidence supports a dual sensory-motor role for insect wings. Dryad Digital Repository. (http://dx.doi.org/10.5061/dryad.7hm1m)

APPENDIX B

Asymmetries in Wing Inertial and Aerodynamic Torques Contribute to Steering in Flying Insects

Mark Jankauski*, T.L. Daniel, I.Y. Shen

University of Washington, Seattle, WA

Initial Revision: February 16, 2017

Abstract

Maneuvering in both natural and artificial miniature flying systems is assumed to be dominated by aerodynamic phenomena. To explore this, we develop a flapping wing model integrating aero and inertial dynamics. The model is applied to an elliptical wing similar to the forewing of the Hawkmoth *Manduca sexta* and realistic kinematics are prescribed. We explore critically the stroke deviation phase, as it relates to firing latency in airborne insect steering muscles which has been correlated to various aerial maneuvers. We show that the average resultant force production acting on the body largely arises from wing pitch and roll and is insensitive to the phase and amplitude of stroke deviation. Inclusion of stroke deviation can generate significant averaged aerodynamic torques at steady-state and adjustment of its phase can facilitate body attitude control. Moreover, wing angular momentum varies with stroke deviation phase, implying a non-zero impulse during a time-dependent phase shift. Simulations show wing inertial and aerodynamic impulses are of similar magnitude during short transients whereas aerodynamic impulses dominate during longer transients. Additionally, inertial effects become less significant for smaller flying insects. Body yaw rates arising from these impulses are consistent with biologically measured values. Thus, we conclude (1) modest changes in stroke deviation can significantly affect steering and (2) both aerodynamic and inertial torques are critical to maneuverability, the latter of which has not widely been considered. Therefore, the addition of a control actuator modulating stroke deviation may decouple lift/thrust production from steering mechanisms and provide inertial shaping benefits in flapping wing micro aerial vehicles.

*Email address: mjankaus@uw.edu

1 Introduction

Over the past decade, micro air vehicles (MAVs) have garnered significant interest in engineering and biology communities. Boasting compact size and maneuverability, MAVs are ideal candidates for applications in infrastructure monitoring and reconnaissance/surveillance missions. To meet the demands of these applications, there have been appreciable efforts made to reduce the length scale of these vehicles without sacrificing performance. However, as MAVs are reduced to the scale of an insect, traditional fixed rotor designs become infeasible because viscous stresses dominate lift and thrust production and rotary motors become inefficient owing to substantial energy losses [1–3]. At such small scales, novel aerodynamic mechanisms associated with flapping wing motions [4] provide mechanisms for lift that are unavailable to rotary systems. Thus, researchers continue to focus their attention on flapping wing flight for small vehicle scales.

In the development of flapping wing micro air vehicles (FWMAVs), flying insects frequently serve as inspiration for engineered designs. The mechanics of wings, the mechanisms of actuation, energy storage, and sensorimotor control have all provided guidance for a range of engineered systems. For instance, the Harvard Robobee, boasting a total mass of 80 mg and wingspan of only 3 cm, was designed using the Diptera (true flies) as inspiration [5]. The robot is supplied power through tethers and is most reliably controlled using off board visual tracking. Creating a robot at this scale is accompanied by significant engineering challenges, largely due to reduced payload capacity. Both actuators and on-board sensors constitute a substantial percentage of the total vehicle weight and power consumption. Thus, there is a necessity for actuator/sensor optimization to reduce FWMAV mass and lower energetic flight requirements.

In an effort to improve the actuator/sensor packages found of FWMAVs, several researchers have sought to characterize the remarkably complex locomotion of flapping wing insect flight. Insects are extraordinarily adept fliers that have the ability to hover and perform aggressive aerial maneuvers [6]. In most insects, the gross wing motion is generated by two sets of primary flight muscle sets in the thoracic cavity, termed dorsal longitudinal muscles (DLMs) and dorso-ventral muscles (DVMs) [7]. These muscles deform the thorax and, through a complex wing hinge system, indirectly actuate wings [8]. The DLMs drive wing down-strokes whereas the DVMs drive wing elevation. There is recent evidence that some control authority resides in these powerful flight muscles [9]. However, the dominant paradigm for control is thought to be relegated to small steering muscles that modify the wing trajectory by changing the articulation of the wing hinge, with the DLMs and DVMs providing the bulk of the power. This unique anatomical structure gives rise to an appealing hypothesis – perhaps gross wing motion is controlled by the power flight muscles whereas steering muscles fine-tune wing kinematics to induce aerial maneuvers. This deconvolution of power production and control may inform the design of FWMAV drive trains, where a set of power actuators can be used to govern

primary wing motion and a smaller set of control actuators can be used to adjust vehicle attitude.

There exists a plethora of observational evidence in biology that strongly correlates steering muscle activity to various changes in body orientation. For instance, bilateral actuation of the third axillary muscles (3AXM) in moths has been found to adjust body pitch angle [10, 11]. Asymmetric stimulation of the 3AXM muscle in beetles in free flight was found to induce banked turns [12]. Balint and Dickinson [13] observed steering muscle activity correlated to variations in the stroke deviation angle in blowflys. Similarly, variant steering muscle firing patterns were found to modulate stroke deviation in hawkmoths [11]. By extension, it seems steering muscles and consequently the stroke deviation angle have pronounced influence on body attitude.

The literature aerodynamic models describe the complex unsteady flow past flapping wings [14–16]. These models have been used to describe various aerial maneuvers, claiming shifts in the wings pressure center relative to the insect center of mass can be used to pitch the insect body forward, for example. However, these models often neglect the stroke deviation angle [17, 18], and the role of inertial moments on the insect body orientation has not been explored in great detail. There exist at least some biological precedents which suggest inertial forces facilitate posture control in various organisms. For example, bats are believed adjust their heading angle by creating imbalances in inertial forces between their wings [19]. Dyhr et al. concluded abdominal flexion in the Hawkmoth *Manduca sexta* can effectively redirect lift forces [20]. Thus, there exists at least some evidence that inertial forces can play an important role in airborne insect steering – the relative role of inertial and aerodynamic forces that arise from changes in stroke deviation remains unexplored.

This paper examines the effect the stroke deviation angle has on net torque production during turning. To do so, a simple model that integrates aerodynamic and inertial dynamics of two rigid wings rotating about a single fixed point is developed. The effect stroke deviation phase has on net force and moment production is explored in depth. Temporal shifts in stroke deviation phase are looked at such that aerodynamic and inertial impulses and insect body yaw rate can be compared for various timed phase transitions. Finally, the results are compared to observational results in biology and some concluding remarks are made on how these findings may benefit FWMAV drive-train and control system design.

2 Methods

We establish an idealized relationship between two wings and the insect body, leveraging a wing-bound reference frame to prescribe kinematics to a rotating insect wing. Inertial moments are derived through the wing angular momentum. A simplified blade element aerodynamic model is introduced to estimate aerodynamic forces and moments. The integrated aerodynamic/inertial model is linearized about the infinitesimal stroke

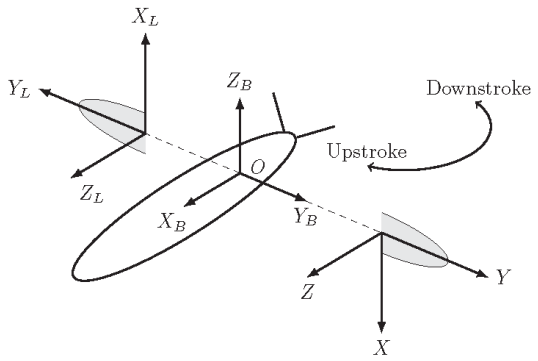

Figure 1: Inertial reference frames for left wing, right wing and insect body. Left wing inertial frame is denoted $X_L Y_L Z_L$, right wing inertial frame is denoted XYZ, and insect body inertial frame is denoted $X_B Y_B Z_B$. The right wing and insect inertial body frames are related by $X = -Z_B$, $Y = Y_B$, $Z = X_B$. Wings are shown offset from the insect body for clarity. Direction of upstroke and downstroke noted on figure. Insect body and wings not drawn to scale.

deviation angle such that order analysis can be employed.

2.1 Reference Frames and Wing Kinematics

Two wings attach to an insect body body at a fixed point O (Fig. 1). This idealization estimates how wing forces and moments are transmitted to the insect body. Given that O is a fixed point, this configuration resembles hovering flight. Other flight regimes, such as forward flight, require O to move with the insect body. The causes additional velocity/acceleration terms associated with body translation which affect the net forces and torques (both aerodynamic and inertial) acting at body reference point O. Owing to the increased complexity of forward flight, we focus on hovering flight in this work. For brevity, the equations of motion are formulated only for the right wing. Symmetry arguments are employed to determine how the moments and forces generated by the left wing affect the net moments and forces acting on the body at fixed point O.

Then, a non-inertial wing-fixed xyz reference frame rotating about fixed point O is established (Fig. 2). We employ Tait-Bryan angles rather than Euler angles, where the rotation convention is represented by $(X - y'' - z')$ and rotations occur about three explicitly distinct axes. The angular velocity $\vec{\Omega}$ of the wing-fixed reference frame is expressed as

$$\vec{\Omega} = \dot{\alpha}\hat{e}_{x''} + \dot{\beta}\hat{e}_{y'} + \dot{\gamma}\hat{e}_z \tag{1}$$

where $\hat{e}_n$ represents a unit vector in the n direction. We relate unit vectors in intermediate coordinate frames to unit vectors in the wing-fixed xyz reference frame such that $\vec{\Omega}$ can be represented in terms of $\hat{e}_x - \hat{e}_y - \hat{e}_z$. After relating unit vectors, the angular velocity becomes

$$\vec{\Omega} = \underbrace{(\dot{\alpha}\cos\beta\cos\gamma + \dot{\beta}\sin\gamma)}_{\omega_x}\hat{e}_x + \underbrace{(\dot{\beta}\cos\gamma - \dot{\alpha}\cos\beta\sin\gamma)}_{\omega_y}\hat{e}_y + \underbrace{(\dot{\gamma} + \dot{\alpha}\sin\beta)}_{\omega_z}\hat{e}_z \tag{2}$$

Determining quantities (angular momentum, aerodynamic moments, etc.) in the fully rotated coordinate frame is relatively straightforward, whereas doing so in the inertial reference frame is challenging. However, in order to understand the relative forces/moments acting on the insect body, it is more appropriate to represent quantities in a fixed inertial frame. An arbitrary vector quantity $\vec{A}$ can be represented in the inertial frame by the transformation

$$(\vec{A})_{XYZ} = \mathbf{R}^T(\vec{A})_{xyz} \tag{3}$$

where the rotation matrix $\mathbf{R}$ is given by

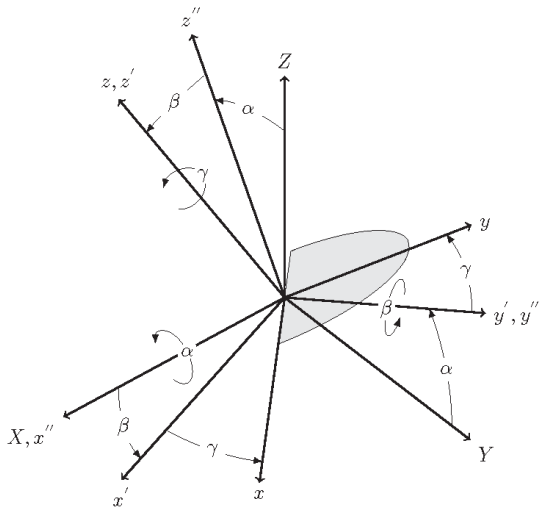

Figure 2: Wing-fixed reference frame. The right wing inertial reference frame (XYZ) is rotated about the positive X axis by an amplitude α, where α denotes wing roll. The subsequent reference frame ($x''y''z''$) is rotated about the positive y'' axis by an amplitude β, where β denotes wing pitch. A final rotation of amplitude γ occurs about the positive z' axis in the $x'y'z'$ frame, where γ represents the stroke deviation angle. The terminal wing-fixed reference frame is denoted xyz

$$\mathbf{R} = \mathbf{R}_z \mathbf{R}_{y'} \mathbf{R}_{x''} \tag{4}$$

$$\mathbf{R}_{x''} = \begin{bmatrix} 1 & 0 & 0 \\ 0 & \cos\alpha & \sin\alpha \\ 0 & -\sin\alpha & \cos\alpha \end{bmatrix} \quad \mathbf{R}_{y'} = \begin{bmatrix} \cos\beta & 0 & -\sin\beta \\ 0 & 1 & 0 \\ \sin\beta & 0 & \cos\beta \end{bmatrix} \quad \mathbf{R}_z = \begin{bmatrix} \cos\gamma & \sin\gamma & 0 \\ -\sin\gamma & \cos\gamma & 0 \\ 0 & 0 & 1 \end{bmatrix} \tag{5}$$

For convenience, all quantities derived in the theory section will be done so in the wing-fixed xyz reference frame. All quantities are converted to the XYZ inertial reference frame in the results section.

2.2 Inertial and Aerodynamic Moments and Impulses

Derivation of the angular momentum and moments for a rigid body rotating about a fixed point in three-dimensions is well understood. Within the rotating reference frame, the angular momentum $\vec{H}_0$ for a single wing is expressed as

$$\vec{H}_0 = \mathbf{I}_0 \vec{\Omega} \tag{6}$$

where $\mathbf{I}_0$ is the inertial tensor, which is constant with respect to the body-fixed coordinate system. Assuming the wing to be a flat, planar structure with negligible thickness, the inertial tensor $\mathbf{I}_0$ can be expressed as

$$\mathbf{I}_0 = \begin{bmatrix} I_{xx} & -I_{xy} & 0 \\ -I_{xy} & I_{yy} & 0 \\ 0 & 0 & I_{zz} \end{bmatrix} \tag{7}$$

where I_{xx}, I_{yy} and I_{zz} are the moments of inertia about the x, y and z axes respectively and I_{xy} is the product of inertia relative to the $x-y$ plane. The inertial moments are then determined by differentiating the angular momentum with respect to time, resulting in

$$\vec{M}_{0,inertial} = \vec{\Omega} \times \mathbf{I}_0 \vec{\Omega} + \mathbf{I}_0 \dot{\vec{\Omega}} \tag{8}$$

For conciseness, these moments will be referred to as the inertial moments throughout the remainder of the paper to differentiate them from aerodynamic moments.

Next, we develop expressions for the aerodynamic moments acting on the wing. Owing to complex unsteady flows [4], the aerodynamic forces and moments are somewhat more difficult to estimate than the inertial moments derived above. While computational fluid dynamics (CFD) has been used with some success

to quantify aerodynamic forces and moments, the method is computationally expensive and not conducive to parametric studies [15]. Instead we rely on a simpler, albeit approximate, Blade Element Momentum Theory (BEMT) that has been used with some success in earlier studies [21–23]. The method functions by discretizing a wing into infinitesimal airfoils. Local aerodynamic forces and moments acting on each foil are determined and then integrated to determine the net aerodynamic force and moment acting over the entire wing. While BEMT assumptions typically ignore critical aerodynamic phenomena such as leading edge vortices, spanwise flows and wing-wake interactions, the method provides reasonable order-of-magnitude estimates of aerodynamic forces and moments. Thus, while higher fidelity models (e.g. CFD) may reveal fundamental aerodynamic mechanisms giving rise to observed flows and force coefficients, the literature does not suggest that such approaches will significantly alter our conclusions. The advantage of the reduced-order BEMT model lies in the ease which one can estimate forces and torques over a wide range of parameter values; the disadvantage lies in the extend to which such models approximate real flow dynamics.

Several BEMT models are readily available, and as a result, the theoretical derivation presented here is brief [17, 24, 25]. However, due to the assumed reference frame kinematics corresponding wing orientation, individual aerodynamic terms used in this model deviate from those presented by other researchers [18]. For a more thorough treatment of each aerodynamic term considered, the reader is encouraged to refer to Appendix A. In general, the formulation for BEMT states

$$dF = Cq\,dS \tag{9}$$

where dF is a differential force acting on the discrete airfoil, C is an non-dimensional empirically measured aerodynamic coefficient, q is the dynamic pressure acting on the airfoil, and dS is a differential reference area. In general, aerodynamic coefficients are determined using dynamically-scaled robotic flappers. For example, Dickinson et al. calculated lift and drag coefficients by rotating a scaled wing in mineral oil, varying the effecting angle of attack between subsequent experiments [26]. This methodology has been used with success to determine other empirical coefficients, such as the coefficient of rotational damping. We draw upon available empirical coefficients for our own model. Then, dynamic pressure is defined by

$$q = \frac{1}{2}\rho_f \vec{V} \cdot \vec{V} \tag{10}$$

where ρ_f is the fluid density and $\vec{V}$ is the instantaneous fluid velocity vector varying along a reference line. The differential reference area dS is defined by

$$dS = c(r)dr \tag{11}$$

where $c(r)$ is the chord-width along the wing referenced from reference axis r (Fig. 4). Reference axis r is used to estimate the instantaneous fluid velocity at each discrete airfoil, and because r is coincident with y, all fluid velocity components are acting in-plane to each airfoil. Then, the position of each point on the wing along a reference line r can be described by $\vec{r} = r\hat{e}_y$. Differentiating the position yields the velocity of each point along the reference line as

$$\vec{V} = r(\vec{\Omega} \times \hat{e}_y) = \underbrace{-r\omega_z}_{v_x}\hat{e}_x + \underbrace{r\omega_x}_{v_z}\hat{e}_z \tag{12}$$

Differentiating the velocity with respect to time yields the acceleration of each point along the reference line

$$\vec{a} = r[\vec{\Omega} \times (\vec{\Omega} \times \hat{e}_y) + \dot{\vec{\Omega}} \times \hat{e}_y] = \underbrace{r(\omega_x\omega_y - \dot{\omega}_z)}_{a_x}\hat{e}_x - \underbrace{r(\omega_x^2 + \omega_z^2)}_{a_y}\hat{e}_y + \underbrace{r(\omega_y\omega_z + \dot{\omega}_x)}_{a_z}\hat{e}_z \tag{13}$$

As most aerodynamic forces are dependent only on velocity, the acceleration described above is only necessary when considering added mass. The angle of attack, denoted by AoA, is defined as the angle between the instantaneous fluid velocity and the positive x axis (Fig. 3). The instantaneous fluid velocity, induced solely by the motion of the wing in hover, is a vector equal in magnitude and opposite in direction to the referenced wing velocity $\vec{V}$. The angle of attack is important, as most empirically measured coefficients such as lift and drag coefficients vary significantly with the angle of attack. Mathematically, it takes the form

$$AoA = \tan^{-1}\left(\frac{v_z}{v_x}\right) = \tan^{-1}\left(\frac{-r\omega_x}{r\omega_z}\right) = \tan^{-1}\left(-\frac{\omega_x}{\omega_z}\right) \tag{14}$$

When solving for AoA computationally in Matlab, the atan2 function is used in lieu of the atan function. Then, the total aerodynamic moments acting at fixed point O are given by

$$\vec{M}_{0,aero} = \int_0^R [\vec{r} \times (d\vec{F}_{A,x} + d\vec{F}_{N,z} + d\vec{F}_{AM,z}) + d\vec{M}_{PM,y} + d\vec{M}_{RD,y} + d\vec{M}_{AM,y}]\, dr \tag{15}$$

where $\vec{F}_{A,x}$ is the axial aerodynamic force, $d\vec{F}_{N,z}$ is the normal aerodynamic force, $\vec{F}_{AM}$ is the added mass force, $\vec{M}_{PM,y}$ is the aerodynamic pitching moment, $\vec{M}_{RD,y}$ is the pitching rotational damping, and $\vec{M}_{AM,y}$ is the added mass pitching moment (Fig. 3). Each aerodynamic force/moment term is derived using Eq. 9 as a basis; details of each term are found in Appendix A.

Lastly, angular momentum and net moments are related by the angular impulse $\vec{J}$, defined by $\vec{J} =$

$\int_{t_1}^{t_2} \vec{M}_0\, dt$. The angular impulse serves as a convenient quantity when comparing aerodynamic and inertial moments over a period of time. The angular momentum and moments are related via the impulse-momentum equation

$$\int_{t_1}^{t_2} \vec{M}_{0,total}\, dt = \Delta \vec{H}_0 \tag{16}$$

where $\vec{M}_{0,total}$ is the difference of aerodynamic and inertial moments, $\vec{M}_{0,total} = \vec{M}_{0,aero} - \vec{M}_{0,inertial}$. The angular impulse will be abbreviated to impulse throughout this paper.

2.3 Linearization

In general, the stroke deviation amplitude is much smaller than the amplitude of pitch and roll rotations in flying insects [27]. As a result, it is possible to linearize all terms described above about an operating point $(\gamma, \dot{\gamma}, \ddot{\gamma}) = (0, 0, 0)$, effectively reducing the stroke deviation to an infinitesimal rotation. Linearization allows us to carry out order analysis of each term, assuming finite rotations pitch and roll are of $\mathcal{O}(0)$ and the infinitesimal stroke deviation is of $\mathcal{O}(1)$. We hypothesize the zeroeth order terms arise from primary flight muscles whereas first order terms are a result of the finer steering muscles modulating stroke deviation. This hypothesis is appealing, as steering muscles constitute only a fraction of the total muscle mass, which implies they are capable of producing lesser resultant moments than the larger power muscles [27].

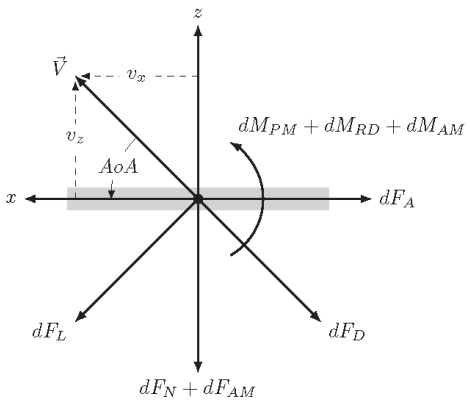

Figure 3: Differential aerodynamic forces and moments from Eq. 35 acting on discrete airfoil. $\vec{V}$ shows the instantaneous velocity of the discrete airfoil referenced from r, and v_x, v_y are the x and y components of instantaneous velocity. Differential drag dF_D acts collinear to $\vec{V}$ and differential lift dF_L acts perpendicular to $\vec{V}$.

The linearization of each term can be conducted by using a Taylor series expansion centered at the operating point $(\gamma, \dot{\gamma}, \ddot{\gamma}) = (0, 0, 0)$. As the expansion of each term can be somewhat arduous, the linearized form of each term is not presented in this paper – a complete version of linearization methods is found in Appendix B. Instead, the linearized lift will serve as an example for the linearization of the other terms. The lift linearized about the operation point is equal to

$$F_L \approx \frac{1}{2}\rho_f \int_0^R r^2 c(r) dr * \left[\underbrace{C_L V^2}_{\mathcal{O}(0)} + \underbrace{\sum_{i=1}^{2} \left(2C_L \left(v_x \frac{\partial v_x}{\partial \gamma^{(i)}} + v_z \frac{\partial v_z}{\partial \gamma^{(i)}} \right) + \frac{\partial C_L}{\partial AoA} \left(\frac{\partial v_z}{\partial \gamma^{(i)}} v_x - \frac{\partial v_x}{\partial \gamma^{(i)}} v_z \right) \right) \gamma^{(i)}}_{\mathcal{O}(1)} \right]_{\gamma, \dot{\gamma}=0} + \mathcal{O}(2) \quad (17)$$

where $\gamma^{(1)} = \gamma$ and $\gamma^{(2)} = \dot{\gamma}$. Note that lift is not a function of $\ddot{\gamma}$, and therefore need not be linearized about $\ddot{\gamma} = 0$. The inertial moments and added mass terms, on the other hand, will require further linearization about $\ddot{\gamma} = 0$. It should also be stressed that the rotation matrix $\mathbf{R}$ will have to be linearized as well when representing quantities in the inertial frame.

3 Results

Idealized wing geometry and simulation parameters are introduced. We then explore the effect stroke deviation angle has on net force and moment production. Averaged wing angular momentum is calculated as a function of stroke deviation phase. A timed shift in deviation phase is presented and aerodynamic impulses are compared with inertial impulses during this transient period.

It is emphasized that all simulation results presented are for a single representative insect wing with a relatively rigid set of kinematics. Therefore, while the results presented provide insight into the functional role of the stroke deviation, they should be extended to other insects/FWMAVs with caution. It is necessary to consider varying wing geometries and kinematics coupled with experimental validation to consider these results universal.

3.1 Simulation Parameters

We model an idealized wing as an planar semi-ellipse identical to the geometry presented by Berman and Wang [23]. Wing thickness is neglected, as thickness is generally much less than the wing span or chord

width. We select an appropriate surface area density ρ_s such that total wing mass agrees with reported measured values. Then, wing chord width $c(r)$ can be expressed via an analytic function

$$c(r) = \frac{4\bar{c}}{\pi}\sqrt{1 - \frac{r^2}{R^2}} \tag{18}$$

where $\bar{c}$ is the mean chord width defined by $\bar{c} = \frac{\pi}{2b}$, b is the semi-minor axis of the ellipse and R is the total length of the wing (the semi-major axis of the ellipse). All wing dimensions and simulation parameters are summarized in Table 1. The wing geometry is identical to that presented by Berman et al. [23] and are similar to those found by Hedrick et al [22] for the Hawkmoth *Manduca sexta*. The wing is discretized into 1000 evenly spaced blade elements. Aerodynamic coefficient and rotation profiles are specified. Aerodynamic coefficients are taken from Whitney et al. [18]. Rotations are assumed harmonic functions of the form $n = n_0 \sin(\omega t + \phi_n)$, where n is a place holder for α, β, γ, the flap frequency of the wing is ω and ϕ_n represents a phase shift. Values for the rotation parameters are approximated from values published by Wilmott and Ellington [27].

All numerical results shown are solved via Matlab. Force, moment and momentum terms are solved over a single wing beat period T using 1000 evenly spaced time steps unless otherwise specified. All integration (both spatial and temporal) is conducted numerically using trapezoidal integration. Spatial integration is conducted outside any timing loop to reserve computational power to facilitate large parameter sweeps.

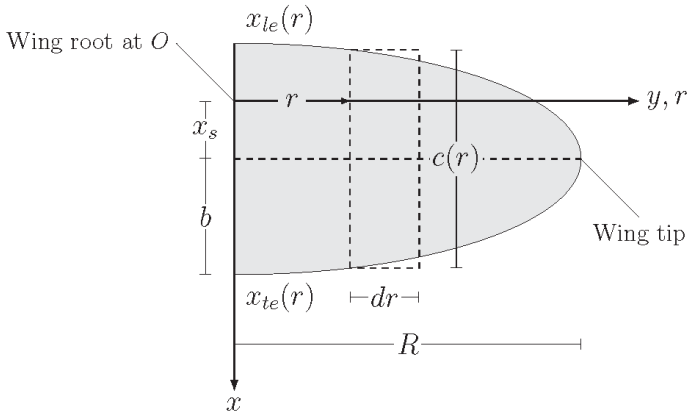

Figure 4: Schematic of wing with dimension definitions. Upper edge of the wing is leading edge $x_{le}(r)$, lower edge of the wing is trailing edge $x_{te}(r)$. Wing root is at fixed point of rotation O. Variable x_s represents a shift of the major axis of the semi-ellipse along the x direction. For the simulation, $x_s = b$ such that the leading edge is coincident with the wing root when $r = 0$. Under this configuration, the wing is recessed behind the pitching y axis of rotation.

Table 1: Summary of Simulation Parameters

Variable	Description	Value	Unit
R	Wing Span	51.9	mm
b	Maximum Chord Width	11.62	mm
x_s	Shift along x axis	11.62	mm
$\bar{c}$	Mean Chord Width	18.26	mm
A	Surface Area	947.7	mm^2
m_w	Wing Mass	47	mg
m	Insect Body Mass	1.648	g
ρ_f	Fluid Density	1.29	kg/m^3
$C_{L,max}$	Max Lift Coefficient	1.8	-
$C_{D,max}$	Max Drag Coefficient	3.4	-
$C_{D,0}$	Min Drag Coefficient	0.4	-
C_{rd}	Rotational Damping Coefficient	5	-
α_0	Roll Amplitude	60	degrees
β_0	Pitch Amplitude	45	degrees
γ_0	Stroke Deviation Amplitude	10	degrees
ϕ_α	Roll Phase	0	rad
ϕ_β	Pitch Phase	$\pi/2$	rad
ϕ_γ	Stroke Deviation Phase	Variable	rad
f	Flap Frequency	25	Hz
I_{xx}	MOI about x	31.65	g-mm^2
I_{yy}	MOI about y	7.88	g-mm^2
I_{zz}	MOI about z	39.46	g-mm^2
I_{xy}	$x-y$ Product of Inertia	11.98	g-mm^2

3.2 Aerodynamic Forces

We first investigate the aerodynamic forces generated by the flapping wing. Note the relationship between the right wing inertial frame XYZ and the insect body frame $X_BY_BZ_B$ (Fig. 1). Hovering implies the upward average net vertical force is equal in magnitude to the downward average net vertical force from aerodynamic,

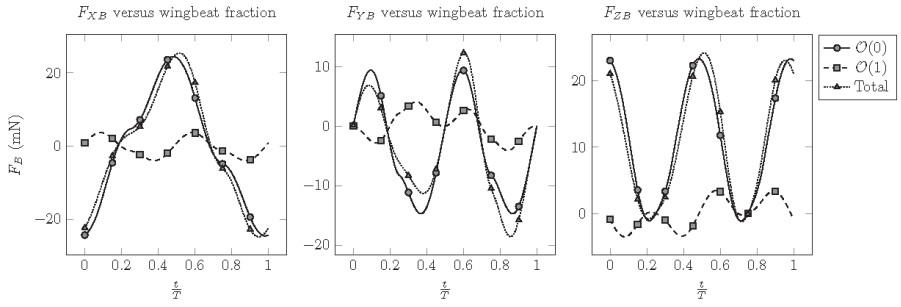

Figure 5: Body forces from single wing versus wingbeat fraction. Zeroeth order, first order and total aerodynamic forces when $\phi_\gamma = \pi/2$.

inertial and gravity forces. Initially, the stroke deviation γ is set to zero, and the phase of pitch ϕ_β is varied from 0 to 2π. In the absence of stroke deviation, only terms of $\mathcal{O}(0)$ are present. The vertical force from the single wing is averaged over a single wing beat period to determine the mean vertical force and doubled to account for the left wing which is assumed to flap symmetrically. Inertial reaction forces are not considered, as they tend to average to zero over the entire parameter space. Given the fixed rotation amplitudes (Tab. 1), maximum mean vertical force was achieved at a pitch phase in the neighborhood of $\phi_\beta = \pi/2$ – mean vertical force was 25% greater in magnitude than the total insect weight. This phase relationship between pitch and roll is consistent with that presented by Berman and Wang [23] and is maintained for the remainder of the paper.

Next, stroke deviation is included at amplitude $\gamma_0 = 10^\circ$ and ϕ_γ is varied from 0 to 2π to determine its effect on aerodynamic force production. Figure 5 shows the total aerodynamic forces over a wingbeat period when $\phi_\gamma = \pi/2$. From the figure, it is apparent the average vertical force stems almost entirely from zeroeth order terms, while first order terms associated with stroke deviation average to nearly zero. Across the entire range ϕ_γ, forces associated with stroke deviation were found to constitute maximally 0.2% of total averaged vertical force. Additionally, stroke deviation did not significantly affect lateral averaged forces in the body X_B or Y_B directions.

This result provides compelling insight into the role of power muscles and steering muscles in flying insects. We hypothesize power muscles dominate aerodynamic force production, which implies steering muscles associated with stroke deviation must serve some other functional role. To expound the role of the stroke deviation further, we next address aerodynamic and inertial moments.

3.3 Averaged Moments

In order for a moment to reorient the insect body over the course of several wingbeats, the average value of the moment over that time span must be nonzero. In this section we identify how inertial and aerodynamic moments are affected by the stroke deviation angle.

First, we address symmetry between the left and right wings. Pitch and roll are assumed identical for both wings. Therefore, only the stroke deviation angle is capable of introducing left-right asymmetry. Consequently, the magnitude of the zeroeth order moments about all axes are identical between left and right wings. Moments due to zeroeth order terms about X_L, X and Z_L, Z are equal and opposite, whereas moments about Y_L, Y are additive. Leveraging these symmetry arguments, we can investigate the total moments acting at fixed point O.

Stroke deviation amplitude is fixed to $\gamma_0 = 10^\circ$ and ϕ_γ is varied between 0 and 2π. Aerodynamic

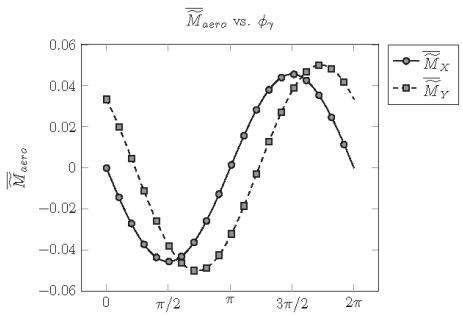

Figure 6: First order non-dimensional averaged aerodynamic moments as a function of ϕ_γ when $\gamma_0 = 10°$. Averaged aerodynamic moments vary linearly with strove deviation amplitude, implying curves double in magnitude when γ_0 is doubled.

and inertial moments are calculated over a single wing beat period and subsequently averaged. Averaged values will be indicated by an overbar. All reported moment values are further non-dimensionalized, first by allowing $\tau = \omega t$ and then by dividing by lead coefficient I_{zz}. Non-dimensionalized values will be denoted by a tilde overscore. Presented moments are with respect to the XYZ right wing inertial frame rather than the body inertial frame.

The simulation shows that inertial moments, both zeroeth and first order, average to zero over a wing beat period. This implies that at steady-state, wing inertial moments do little to reorient the body. Zeroeth order aerodynamic moments about the X and Y axis average to zero. The zeroeth order aerodynamic moment about the Z axis is canceled due to symmetry. Conversely, first order average aerodynamic moments about X and Y vary significantly with ϕ_γ (Fig. 6), while first order aerodynamic moments about Z average to zero over the entire range of ϕ_γ. The averaged pitching moment $\overline{\widetilde{M}}_Y$ in Fig. 6 stems almost entirely from the aerodynamic normal force projected into the inertial wing frame. This projection averages to zero in Y and Z directions, and averages to a non-zero value in the $-X = Z_B$ direction to keep the insect in hover. Consequently, $\overline{\widetilde{M}}_Y$ is contingent on the average wing position in the Z direction ($r\hat{e}_z \times F\hat{e}_x = M\hat{e}_y$). When $\phi_\gamma = \pi/2$, the wing favors the upstroke ($+Z$ direction), causing the body to pitch down. Conversely, if $\phi_\gamma = 3\pi/2$, the wing favors the downstroke ($-Z$ direction), causing the body to pitch up. This trend has been shown experimentally in the fruit flies by Whitehead et al. [28]. Adjustment of the aerodynamic center of pressure $\hat{d}_{cp}$ only modestly affects the results in Fig. 6. A figure investigating the effect of variant $\hat{d}_{cp}$ on averaged aerodynamic moments is available in supplemental material.

Thus, the averaged first order moments show that stroke deviation angle can have a marked effect on steering the insect body, a claim that is well supported by biological evidence. For instance, researchers

have correlated bilateral actuation of the 3AXM muscle (which modulates stroke deviation) to longitudinal pitch control in Hawkmoths [10, 11]. Changes in the body pitch were associated with the firing latency of the 3AXM muscle. While the the muscle firing latency is not fully indicative of stroke deviation phase, there likely exists a correlation between the two. Furthermore, unilateral actuation of the 3AXM muscle causes banked turns in flying beetles [12], and during steady-state rolling maneuvers the blowfly exhibits large phase differences between the strain in some of the left-right steering muscles [29].

Specific to our results, bilateral shifts in stroke deviation phase alter the net mean pitch moment while leaving the net mean roll moment unaffected due to left-right symmetry. The presence of a mean pitching moment implies the center of gravity of the insect must be recessed from the wing axis of rotation – if the center of gravity is coincident with the Y wing axis of rotation, a mean pitch moment would cause the insect to topple end over end. Measurements by Cheng et al. [30] indicate the center of gravity of the Hawkmoth is recessed from the wing axis of rotation by approximately 25% of the total wingspan. It is plausible the mean body pitch angle is prescribed by the equilibrium of the pitching moment due to gravity and the aerodynamic pitching moment caused by the stroke deviation angle. This proves a simple mechanism for controlling body pitch angle via changes in the magnitude and phase of the stroke deviation.

Moreover, the results indicate unilateral phase shifts of the stroke deviation angle can induce banked turns. Should ϕ_γ of the right wing change independently from that of the left wing or visa versa, the result will be a net aerodynamic moment about both wing pitch and roll axes. It is possible to achieve a significant roll moment without a pitching moment, these two axes can be controlled independently. This can be achieved by increasing ϕ_γ of the right wing while subsequently decreasing ϕ_γ of the left wing. The magnitude of the induced moment will then rely on the initial operating phase of the stroke deviation angle. Depending on the magnitude and symmetry of the left-right stroke deviation phase shift, the mean pitching moment may also be maintained during roll maneuvers such that the equilibrium body pitch angle is unaffected.

3.4 Transient Effects

According to our simulation, phase changes in the stroke deviation angle have a substantial impact on the steady-state aerodynamic moments acting on the body. However, there must exist a transient period in which the stroke deviation phase transitions from an initial phase to some final phase. While inertial moments average to zero at steady-state, it is possible they have a larger influence during this transient period. To investigate this, averaged angular momentum of the right wing is calculated as ϕ_γ is varied from 0 to 2π for a fixed amplitude $\gamma_0 = 10^\circ$ (Fig. 7). Clearly, averaged wing angular momentum is sensitive to ϕ_γ. This signifies that during a phase shift from an initial phase ϕ_0 to a final phase ϕ_f, an impulse must have acted

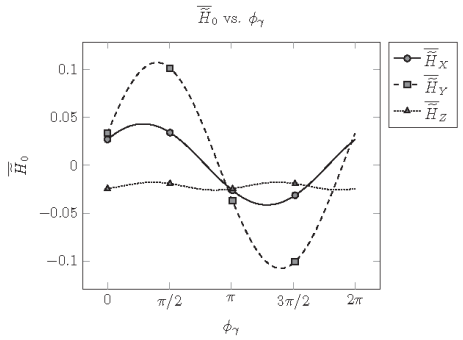

Figure 7: Non-dimensional averaged angular momentum as a function of ϕ_γ

to cause the change of angular momentum. These results motivate a comparison between aerodynamic and inertial impulses during a phase-shifting transient period.

To compare aerodynamic/inertial impulses, a transient function $\phi_\gamma(t)$ is defined with the conditions $\phi_\gamma(0) = \phi_0$ and $\phi_\gamma(NT) = \phi_f$, where N is the number of wing beats during the transient period. As a result, the stroke deviation angle takes the form $\gamma = \gamma_0 \sin[\omega t + \phi_\gamma(t)]$. There are infinitely many transient functions that satisfy initial/final phase conditions, and each unique function may alter the resulting impulses. As an example, linear and fifth-order polynomials are introduced as candidates for $\phi_\gamma(t)$. The fifth-order transient function has the added benefit of being continuous at the $t = 0$ and $t = NT$ in both $\dot{\gamma}$ and $\ddot{\gamma}$, whereas the linear transient function causes discontinuous leaps in stroke deviation velocity and acceleration. Both transient functions and their influence on $\gamma, \dot{\gamma}, \ddot{\gamma}$ are shown in Fig. 8 over a single wingbeat.

Due to the continuity in derivatives of γ, the fifth-order polynomial is used moving forward. An initial phase angle $\phi_0 = 0$ is assumed, and the final phase angle ϕ_f is varied between 0 and 2π in 100 evenly spaced spaced increments. Cases where $N = 1$ and $N = 5$ wingbeats are considered to illustrate how transient duration affects the magnitude of impulses. Impulses are calculated by numerically integrating the moments with respect to time. For the case where $N = 5$, 5000 evenly time steps are used. Zero order impulses are not considered – it is determined that they either integrate to zero or are canceled by wing symmetry. Presented results are again normalized with respect to time and by lead coefficient I_{zz}. The results are shown in Fig. 9. We emphasize the curves represented here will vary with the starting phase ϕ_0.

Simulations suggest an important result – inertial torques may play a critical role in steering. This deviates from the notion that aerodynamic moments dominate body attitude changes in insects. Fig. 9 shows that for short transient periods, the magnitude of inertial impulses is comparable to that of aerodynamic impulses. In some cases, the two impulses act antagonistically thereby decreasing the net impulse acting

on the insect body. Consider the phase shift from $\phi_\gamma = 0$ to $\phi_\gamma = \pi/2$ over a single wingbeat. $J_{Y,aero}$ and $J_{Y,inertial}$ act in opposite directions and have a reducing effect on the total impulse. As a result, the body will have a tendency to pitch about the negative Y axis, which is coincident with Y_B. This might prove to be a novel mechanism to slow the insect body to a halt after an abrupt rotation. It is possible that an insect beginning from rest (zero angular momentum) gains angular momentum during the transient period and then returns to a resting state once the the net impulse has integrated to zero. During other transient phase shifts, aerodynamic and inertial impulses tend to act synergistic.

Moreover, the simulation shows transient timing influences the relative contribution of aerodynamic and inertial torques. The magnitude of aerodynamic impulses increases significantly as transient becomes longer whereas inertial impulses are unaffected; if N is increased beyond 5, aerodynamic impulses completely overwhelm inertial impulses along the X and Y axes. This is likely due to the presence of averaged steady-state aerodynamic moments at different values of ϕ_γ (Fig. 6). This suggests why aerodynamic impulses about Z are insensitive to the transient length – the steady-state aerodynamic moment about Z averages to zero for all stroke deviation phase angles.

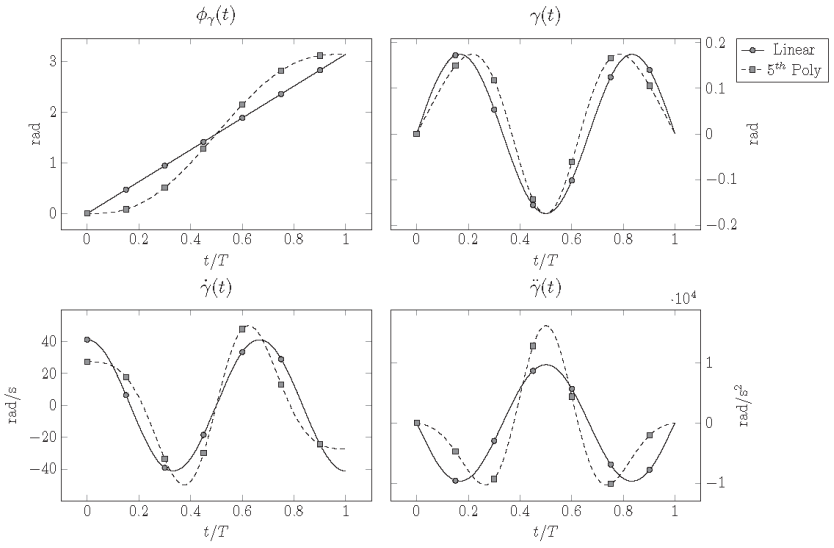

Figure 8: Example transient functions $\phi_\gamma(t)$ and their influence on stroke deviation

3.5 Scaling Effects

For the Hawkmoth *Manduca sexta*, inertial impulses were found comparable in magnitude to aerodynamic impulses during a transient stroke deviation phase shifts. Nonetheless, it is possible the contribution of aerodynamic and inertial impulses varies with the scale of the insect. To assess the scaling effect on aerodynamic/inertial impulses, wings of three different insects are considered – the Hawkmoth, bumblebee and fruitfly. Wing properties are acquired from Berman and Wang [23] and are shown in Table 2. Note the moments of inertia vary slightly from the published values in [23] due to the wing offset x_s.

While aerodynamic coefficients and rotation amplitudes vary modestly for each insect considered, it is convenient to assume uniformity for a more consistent comparison of aerodynamic and inertial impulses.

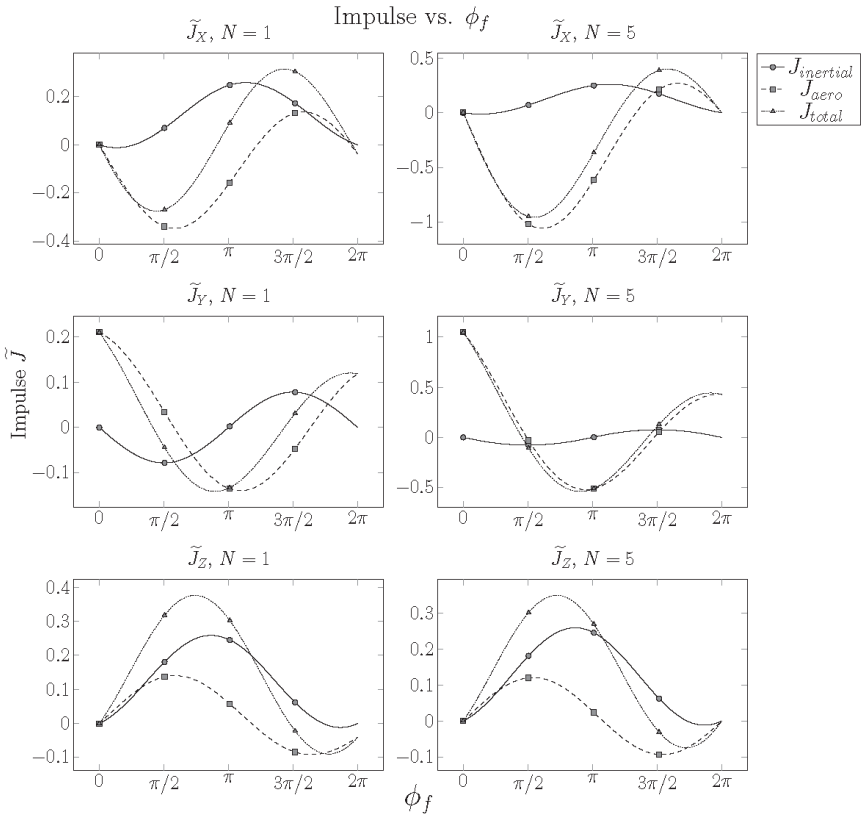

Figure 9: Aerodynamic, inertial and total impulses during transient phase shift from $\phi_0 = 0$ to variable ϕ_f over one and five wingbeats.

Table 2: Wing parameters for Hawkmoth, bumblebee and fruitfly

Parameter	Hawkmoth	Bumblebee	Fruitfly	Unit
R	51.9	13.2	2.02	mm
$\bar{c}$	18.26	4.02	0.67	mm
b	11.62	2.54	0.4265	mm
m_w	47	0.46	8.6×10^{-4}	mg
f	25	116	254	Hz
I_{xx}	31.65	0.0201	8.60×10^{-7}	g-mm^2
I_{yy}	7.88	0.0022	1.82×10^{-7}	g-mm^2
I_{zz}	39.64	0.0222	1.04×10^{-7}	g-mm^2
I_{xy}	11.98	0.0048	2.99×10^{-7}	g-mm^2

Therefore, the rotation amplitudes and aerodynamic coefficients shown in Tab. 1 are used for all three insects. The initial stroke deviation phase is fixed to $\phi_0 = 0$ and the final stroke deviation phase ϕ_f is varied from 0 to 2π in 100 evenly spaced intervals. Owing to the increased flap frequency seen in the bumblebee and fruitfly, 5000 evenly spaced time steps are used for these cases – 1000 evenly spaced time steps are maintained for the Hawkmoth. The aerodynamic and inertial impulses are calculated for each phase transition, where the phase transition occurs over a single wing beat ($N = 1$). Then, the maximum of the absolute value of the each impulse is calculated, and $max|\vec{J}_{inertial}|/max|\vec{J}_{aero}|$ is determined as a function of wing length R. As the maximum values for aerodynamic/inertial impulses likely do not correspond to the same ϕ_f, the RMS values of aerodynamic/inertial impulses over the entire range of ϕ_γ are calculated as well. $rms(\vec{J}_{inertial})/rms(\vec{J}_{aero})$ is also plotted as a function of wing length R. The results are shown in Fig. 10.

This simulation shows that under the given assumptions, inertial effects are less pronounced for smaller flying insects. While not enough data points are considered to identify a clear mathematical trend, it appears the relative contribution of inertial impulses scales non-linearly. In general, inertial moments scale volumetrically, whereas aerodynamic moments scale roughly with the surface area of the wing. However, the uncertainty in scaling stems from uncertainty in the scaling of wing mass and wingbeat frequency. For example, the mass per unit area varies significantly between insects [31], limiting a rigorous scaling analysis. Inertial impulses about Z shows the largest variation for the various insects whereas the variation of inertial impulses about Y is much less. In any case, inertial impulses constitute a large percentage of the total impulse.

3.6 Body Yaw Angular Velocity

Airborne insects achieve considerable angular velocity during aerial maneuvers. For example, the Hawkmoth *Manduca Sexta* has been measured at angular rates as large as $800°/s$ about the body yaw axis [32]. Con-

sequently, it is prudent to assess the achievable angular velocity about at least one axis of the insect body using the model developed in this research.

Body rotations will cause an additional component of velocity to the wing, an effect that is not accounted for in this model. However, the maximum angular velocity of the wing (approximately 9500°/s about the roll axis) is significantly larger than the achievable angular velocity of the body. Therefore, body dynamics will only slightly affect net wing angular velocity and consequently, the net moment production. Thus, we choose to represent an idealized situation in which the body is permitted to rotate independently of the wings. We assume the only moments causing body rotation are the inertial and aerodynamic moments generated by the flapping wings. For this reason, angular velocity about Y_B is not considered. Body pitch angular velocity relies not only on gravity, but also on unmodeled abdominal flexion [33] which may affect net pitching moments. Furthermore, no reliable data was found regarding angular velocity or inertial properties about the body roll axis X_B for the Hawkmoth *Manduca Sexta*. Consequently, only angular velocity about the body yaw axis (Z_B) is considered.

To determine the body yaw angular velocity, we assume the insect body is coincident with the X_B axis. The body is then pinned such that it can rotate only about the Z_B axis. An initial stroke deviation phase ϕ_0 is selected and a timed phase shift to ϕ_f is introduced. The initial stroke deviation phase is set to $\phi_0 = \pi$ for two reasons. First, it represents a zero-crossing of the averaged aerodynamic moments about about X (Fig. 6), which is coincident with yaw body axis Z_B (Fig. 1). Operating at this zero-crossing is beneficial, as a phase advance/delay will correspond to a steady-state positive/negative averaged aerodynamic moment $\widetilde{\overline{M}}_X$. Second, $\phi_0 = \pi$ corresponds to a negative steady-state aerodynamic moment about Y (Fig. 6), representing the case where the averaged aerodynamic moment causes the insect body to be inclined and recessed

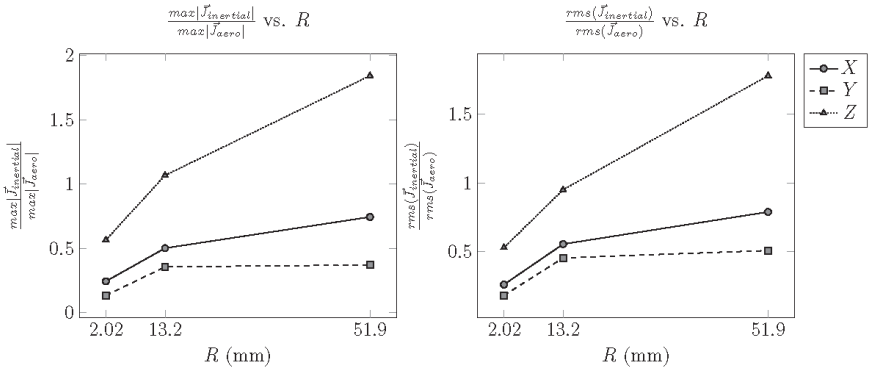

Figure 10: Comparison of aerodynamic and inertial impulses for insect wings of varying length scales.

from the wing leading edge.

With the initial stroke deviation phase ϕ_0 fixed, the final stroke deviation phase ϕ_f is varied from 0 to 2π in 100 evenly spaced increments. Transient durations of one and five wingbeats are considered. The impulse from the total moment during each phase transition is calculated, and the resulting body angular velocity $\omega_{Z,B}$ immediately following the transient is determined using the impulse-momentum relationship in Eq. 16. The insect body starts from rest (no angular momentum) and the insect moment of inertia about the yaw body axis $I_{ZZ,B}$ is taken from Hedrick et al. [32] for a value of $I_{ZZ,B} = 2.43 \times 10^{-7}$ kg-m^2. The achievable body yaw angular velocities from a single wing are shown in Fig. 11. Contributions of inertial and aerodynamic impulses to $\omega_{Z,B}$ are shown separately.

According to the simulation results shown in Fig. 11, the insect can achieve the measured angular body yaw rate of $800°/s$ simply by adjusting the stroke deviation phase – a nontrivial amount of this angular velocity is generated by inertial torques. In the case where $N = 1$, this can be accomplished by advancing ϕ_γ of the right wing from π to approximately $5\pi/4$ while simultaneously reducing ϕ_γ of the left wing from π to $3\pi/4$. For the case where $N = 5$, a much smaller deviation from ϕ_0 can cause the same effect. Larger deviations induce body yaw angular velocities likely not realistic in insect flight. Similar to the inertial moments and impulses shown in Fig. 9, the contribution of aerodynamic moments to $\omega_{Z,B}$ increases with the duration of the phase shift whereas the contribution of inertial moments is unaltered.

4 Discussion

Our simulation results shows that (1) modest changes in stroke deviation induce aerial maneuvers, and (2) inertial torques may play a much more profound role in steering and insect flight control than previously

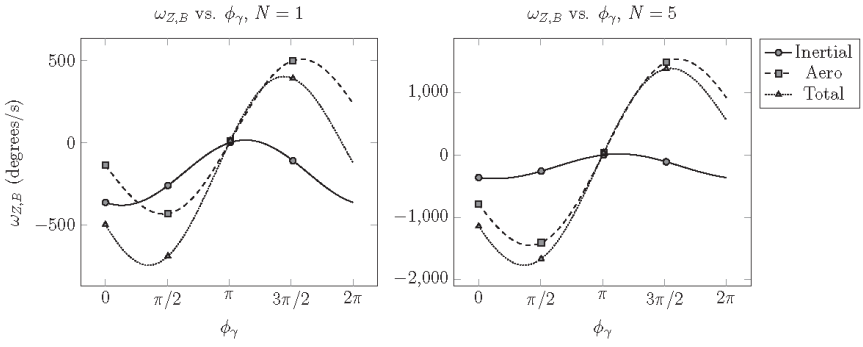

Figure 11: Aerodynamic and inertial contributions from single wing to $\omega_{Z,B}$ and total $\omega_{Z,B}$ immediately after transient phase shift from $\phi_0 = \pi$ to variable ϕ_f over one and five wingbeats.

thought. Both of these key findings have important implications for our understanding of control and dynamics in insect flight and for FWMAVs.

First, FWMAV aerodynamic force production may be decoupled from control. Similar to biological mechanisms, lift/thrust production can be generated through a set of power actuators whereas steering can be relegated to smaller control actuators modulating stroke deviation. Finio et al. [34] suggested such stroke deviation actuators could be implemented on the Harvard Robobee. This design scheme allows power actuators to operate at an optimal frequency and magnitude and not deviate from this set-point to adjust vehicle attitude. This benefit is especially pronounced in the case of PZT actuators, where deviations in driving frequency or magnitude degrade actuator efficiency. Moreover, deviations in power actuator amplitude may adversely affect lift/thrust production – separate control actuators may mitigate this problem. More specifically, active control over the stroke deviation angle allows FWMAVs to conscientiously adjust body pitch angle, a capability many designs do not possess. This is appealing to FWMAVs equipped with optical systems, as it allows vertical inspection objects without changing altitude. Additionally, stroke deviation actuation offers control authority over the wing roll axis, allowing vehicles to adjust course easily.

Perhaps more intriguingly, authority over the stroke deviation angle may facilitate inertial trajectory shaping. Our results show that abrupt changes in stroke deviation phase gives rise to inertial torques on the same order of magnitude as aerodynamic torques. While inertial attitude control has been implemented on larger vehicles [19], such mechanisms have yet to be realized on insect-scale aerial robotics. Such control may dramatically improve dexterity and agility of FWMAVs, with wing angular momentum serving as a quintessential design quantity. Significant efforts must be made to assess the feasibility of inertial control on these micro systems. Stroke deviation actuators may require excessive power to generate the quick phase changes necessary to generate large inertial imbalances. Large inertial torques may cause detrimental stresses on the vehicle airframe.

Nonetheless, while our simulations show promising results, there remains a necessity for model validation. In-vivo experiments are unrealistic due to the requirement of vacuum conditions and highly controlled degrees of freedom. However, there are other mechanisms available for cross-validation. First, we may employ a full-scale fluid-structure coupled simulation. Medium density should be varied systematically and resulting aerodynamic moments monitored to compare the relative magnitudes of inertial and aerodynamic forces. Unfortunately, computational simulation themselves require experimental validation, rendering this approach undesirable. Alternatively, a three degree-of-freedom robotic flapper capable of replicating the complex wing kinematics may developed. Experiments can be conducted in and out of vacuum or in reduced medium density conditions (e.g. helium) so that inertial and and aerodynamic forces can be decoupled. This approach is accompanied by significant design challenges and requires extensive resources. Existing dynamically-scaled

robotic flappers generally operate in mineral oil. Non-dimensional analysis generally produces suitable estimates of fluid forces, but unrealistically high wing densities are required to properly scale inertial forces. As a result, any experiment comparing inertial and aerodynamic mechanisms is best conducted in air or another suitable medium where realistic inertial characteristics can be realized. This is no trivial task – development of a high-frequency 3-axis rotation stage with precision kinematics is a substantial challenge. Thus, we believe the work presented provides an excellent avenue for future research, with the theoretic predictions presented in this paper motivating rigorous experimental work.

5 Conclusion

Insects exhibit a strong correlation between aerial maneuvers and stroke deviation actuation. To investigate the mechanisms underlying this correlation, we developed an integrated aerodynamic/inertial model of flapping wings to predict forces, torques and impulses that arise from stroke deviations. The model is linearized by the small stroke deviation angle such that zeroeth order terms are contingent only on wing pitch and roll whereas first order terms rely on all three rotations. The stroke deviation amplitude is fixed, and the phase is varied to represent changes in insect steering muscle firing latency.

The results elucidate the functional role of the stroke deviation angle, which is strongly correlated to steering muscle activity. The stroke deviation angle has an insignificant effect on aerodynamic force production – rather, lift and thrust largely relied on symmetric wing pitch and roll. Variance of the stroke deviation phase has a large effect on the steady-state averaged aerodynamic moments acting at the fixed point, which are necessary to reorient the insect body. These results corroborate observations in which steering muscle activity was correlated to various aerial maneuvers [11].

The angular momentum of the wing was also found to vary with the stroke deviation phase, motivating a closer look into the transient period during which the stroke deviation varies phase. During the transient period, both inertial and aerodynamic impulses play significant roles, with the latter in growing in magnitude as the duration of the transient period increases. Such a result suggests that, in contrast to prevailing views that only aerodynamic forces are implicated in flight control, inertial moments generated by steering muscles facilitate changes in body orientation, particularly if phase shifts occur on sub wing beat timescales. Simulations show inertial effects become less pronounced for smaller flying insects. Additionally, achievable body yaw rates fell within anatomical limits for most temporal phase shifts.

Finally, insights into how the stroke deviation angle can benefit FWMAV drive-train and control system design were given. The addition of an actuator modulating stroke deviation is purported to decouple lift/thrust production from and steering mechanisms. The benefit of such a deconvolution is the ability to

maintain power actuators at an optimal set point. Thus, power actuators can be utilized to generate gross wing trajectory, whereas smaller control actuators can be used to finely modify wing kinematics thereby inducing aerial maneuvers. These aerial maneuvers can further be refined by leveraging inertial mechanisms arising from quick shifts in stroke deviation phase.

Acknowledgment

This material is based upon work supported by the National Science Foundation under Grant No. CMMI-1360590, and Air Force Office of Scientific Research under grants FA9550-11-1-0155, FA9550-14-1-0398 and FA8651-13-1-0004. Any opinions, findings, and conclusions or recommendations expressed in this material are those of the authors and do not necessarily reflect the views of the National Science Foundation or the Air Force Office of Scientific Research.

References

[1] Umberto Pesavento and Z Jane Wang. Flapping wing flight can save aerodynamic power compared to steady flight. *Physical review letters*, 103(11):118102, 2009.

[2] WSN Trimmer. Microrobots and micromechanical systems. *Sensors Actuators*, 1989.

[3] Sawyer B Fuller, Michael Karpelson, Andrea Censi, Kevin Y Ma, and Robert J Wood. Controlling free flight of a robotic fly using an onboard vision sensor inspired by insect ocelli. *Journal of The Royal Society Interface*, 11(97):20140281, 2014.

[4] Sanjay P Sane. The aerodynamics of insect flight. *Journal of experimental biology*, 206(23):4191–4208, 2003.

[5] Robert J Wood. The first takeoff of a biologically inspired at-scale robotic insect. *Robotics, IEEE Transactions on*, 24(2):341–347, 2008.

[6] Robert C Michelson and Steven Reece. Update on flapping wing micro air vehicle research-ongoing work to develop a flapping wing, crawling entomopter. In *13th Bristol International RPV/UAV Systems Conference Proceedings, Bristol England*, volume 30, pages 30–1, 1998.

[7] Michael H Dickinson and Michael S Tu. The function of dipteran flight muscle. *Comparative Biochemistry and Physiology Part A: Physiology*, 116(3):223–238, 1997.

[8] Tanvi Deora, Amit Kumar Singh, and Sanjay P Sane. Biomechanical basis of wing and haltere coordination in flies. *Proceedings of the National Academy of Sciences*, 112(5):1481–1486, 2015.

[9] Simon Sponberg, Thomas L Daniel, and Adrienne L Fairhall. Dual dimensionality reduction reveals independent encoding of motor features in a muscle synergy for insect flight control. *PLoS Comput Biol*, 11(4):e1004168, 2015.

[10] Noriyasu Ando and Ryohei Kanzaki. Changing motor patterns of the 3rd axillary muscle activities associated with longitudinal control in freely flying hawkmoths. *Zoological science*, 21(2):123–130, 2004.

[11] Hao Wang, Noriyasu Ando, and Ryohei Kanzaki. Active control of free flight manoeuvres in a hawkmoth, agrius convolvuli. *Journal of Experimental Biology*, 211(3):423–432, 2008.

[12] Hirotaka Sato, Tat Thang Vo Doan, Svetoslav Kolev, Ngoc Anh Huynh, Chao Zhang, Travis L Massey, Joshua Van Kleef, Kazuo Ikeda, Pieter Abbeel, and Michel M Maharbiz. Deciphering the role of a coleopteran steering muscle via free flight stimulation. *Current Biology*, 25(6):798–803, 2015.

[13] Claire N Balint and Michael H Dickinson. The correlation between wing kinematics and steering muscle activity in the blowfly calliphora vicina. *Journal of experimental biology*, 204(24):4213–4226, 2001.

[14] Jiang Hao Wu and Mao Sun. Unsteady aerodynamic forces of a flapping wing. *Journal of Experimental Biology*, 207(7):1137–1150, 2004.

[15] Mao Sun and Jian Tang. Lift and power requirements of hovering flight in drosophila virilis. *Journal of Experimental Biology*, 205(16):2413–2427, 2002.

[16] Hikaru Aono, Satish Kumar Chimakurthi, Pin Wu, E Sallstrom, Bret K Stanford, C Cesnik, Peter Ifju, Lawrence Ukeiley, and Wei Shyy. A computational and experimental study of flexible flapping wing aerodynamics. In *48th AIAA aerospace sciences meeting including the new horizons forum and aerospace exposition*, pages 4–7, 2010.

[17] QT Truong, QV Nguyen, VT Truong, HC Park, DY Byun, and NS Goo. A modified blade element theory for estimation of forces generated by a beetle-mimicking flapping wing system. *Bioinspiration & biomimetics*, 6(3):036008, 2011.

[18] JP Whitney and RJ Wood. Aeromechanics of passive rotation in flapping flight. *Journal of Fluid Mechanics*, 660:197–220, 2010.

[19] J Colorado, Antonio Barrientos, Claudio Rossi, and C Parra. Inertial attitude control of a bat-like morphing-wing air vehicle. *Bioinspiration & biomimetics*, 8(1):016001, 2012.

[20] Jonathan P Dyhr, Kristi A Morgansen, Thomas L Daniel, and Noah J Cowan. Flexible strategies for flight control: an active role for the abdomen. *Journal of Experimental Biology*, 216(9):1523–1536, 2013.

[21] Sanjay P Sane and Michael H Dickinson. The aerodynamic effects of wing rotation and a revised quasi-steady model of flapping flight. *Journal of experimental biology*, 205(8):1087–1096, 2002.

[22] Tyson L Hedrick and TL Daniel. Flight control in the hawkmoth manduca sexta: the inverse problem of hovering. *Journal of Experimental Biology*, 209(16):3114–3130, 2006.

[23] Gordon J Berman and Z Jane Wang. Energy-minimizing kinematics in hovering insect flight. *Journal of Fluid Mechanics*, 582:153–168, 2007.

[24] Toshiyuki Nakata, Hao Liu, and Richard J Bomphrey. A cfd-informed quasi-steady model of flapping-wing aerodynamics. *Journal of Fluid Mechanics*, 783:323–343, 2015.

[25] Sanjay P Sane and Michael H Dickinson. The control of flight force by a flapping wing: lift and drag production. *Journal of experimental biology*, 204(15):2607–2626, 2001.

[26] Michael H Dickinson, Fritz-Olaf Lehmann, and Sanjay P Sane. Wing rotation and the aerodynamic basis of insect flight. *Science*, 284(5422):1954–1960, 1999.

[27] Alexander P Willmott and Charles P Ellington. The mechanics of flight in the hawkmoth manduca sexta. i. kinematics of hovering and forward flight. *Journal of Experimental Biology*, 200(21):2705–2722, 1997.

[28] Samuel C Whitehead, Tsevi Beatus, Luca Canale, and Itai Cohen. Pitch perfect: how fruit flies control their body pitch angle. *Journal of Experimental Biology*, 218(21):3508–3519, 2015.

[29] Simon M Walker, Daniel A Schwyn, Rajmund Mokso, Martina Wicklein, Tonya Müller, Michael Doube, Marco Stampanoni, Holger G Krapp, and Graham K Taylor. In vivo time-resolved microtomography reveals the mechanics of the blowfly flight motor. *PLoS Biol*, 12(3):e1001823, 2014.

[30] Bo Cheng, Xinyan Deng, and Tyson L Hedrick. The mechanics and control of pitching manoeuvres in a freely flying hawkmoth (manduca sexta). *Journal of Experimental Biology*, 214(24):4092–4106, 2011.

[31] Ngoc San Ha, Quang Tri Truong, Nam Seo Goo, and Hoon Cheol Park. Relationship between wingbeat frequency and resonant frequency of the wing in insects. *Bioinspiration & biomimetics*, 8(4):046008, 2013.

[32] Tyson L Hedrick, Bo Cheng, and Xinyan Deng. Wingbeat time and the scaling of passive rotational damping in flapping flight. *Science*, 324(5924):252–255, 2009.

[33] Armin J Hinterwirth and Thomas L Daniel. Antennae in the hawkmoth manduca sexta (lepidoptera, sphingidae) mediate abdominal flexion in response to mechanical stimuli. *Journal of Comparative Physiology A*, 196(12):947–956, 2010.

[34] Benjamin M Finio, John P Whitney, and Robert J Wood. Stroke plane deviation for a microrobotic fly. In *Intelligent Robots and Systems (IROS), 2010 IEEE/RSJ International Conference on*, pages 3378–3385. IEEE, 2010.

[35] William B Dickson, Andrew D Straw, Christian Poelma, and Michael H Dickinson. An integrative model of insect flight control. In *Proceedings of the 44th AIAA Aerospace Sciences Meeting and Exhibit*, pages 31–38, 2006.

DISTRIBUTION LIST

AFRL-RW-EG-TR-2018-079

Copies to

DEFENSE TECHNICAL INFORMATION CENTER - 1 Electronic Copy (1 file & 1 format)
ATTN: DTIC-OCA (ACQUISITION)
8725 JOHN J. KINGMAN ROAD, SUITE 0944
FT. BELVOIR VA 22060-6218

Kevin Brink, RWWI

Will Curtis, RWWN

Ben Dickinson, RWWN

Kaitlin Fair, RWWI

TJ Klausutis, RWW

Nick Rummelt, RWWI

Jennifer Talley, RWWI

Tony Thompson, RWWG

Ric Wehling, RWWI

Dr Pat Bradshaw, AFOSR/RTB

Tom Daniel, U WA

Johnny Evers, RW Emeritus

Sean Humbert, Univ Colorado, Boulder

Holger Krapp, Imperial College, UK